7476–7493 *Nucleic Acids Research, 2019, Vol. 47, No. 14* *Published online 12 June 2019*
doi: 10.1093/nar/gkz524

Metal sensing and regulation of adaptive responses to manganese limitation by MtsR is critical for group A streptococcus virulence

Hackwon Do[1], Nishanth Makthal[1], Pete Chandrangsu[2,3], Randall J. Olsen[1,4], John D. Helmann[2], James M. Musser[1,4] and Muthiah Kumaraswami[1,*]

[1]Center for Molecular and Translational Human Infectious Diseases Research, Houston Methodist Research Institute, and Department of Pathology and Genomic Medicine, Houston Methodist Hospital, Houston, TX 77030, USA, [2]Department of Microbiology, Cornell University, Ithaca, NY 14853-8101, USA, [3]W.M. Keck Science Department, Claremont McKenna, Pitzer and Scripps College, Claremont, CA 91711, USA and [4]Department of Pathology and Laboratory Medicine, Weill Medical College of Cornell University, New York, NY 10021, USA

Received March 26, 2019; Revised May 29, 2019; Editorial Decision May 31, 2019; Accepted June 03, 2019

ABSTRACT

Pathogenic bacteria encounter host-imposed manganese (Mn) limitation during infection. Herein we report that in the human pathogen *Streptococcus pyogenes*, the adaptive response to Mn limitation is controlled by a DtxR family metalloregulator, MtsR. Genes upregulated by MtsR during Mn limitation include Mn (*mtsABC*) and Fe acquisition systems (*sia* operon), and a metal-independent DNA synthesis enzyme (*nrdFEI.2*). To elucidate the mechanism of metal sensing and gene regulation by MtsR, we determined the crystal structure of MtsR. MtsR employs two Mn-sensing sites to monitor metal availability, and metal occupancy at each site influences MtsR regulatory activity. The site 1 acts as the primary Mn sensing site, and loss of metal at site 1 causes robust upregulation of *mtsABC*. The vacant site 2 causes partial induction of *mtsABC*, indicating that site 2 functions as secondary Mn sensing site. Furthermore, we show that the C-terminal FeoA domains of adjacent dimers participate in the oligomerization of MtsR on DNA, and multimerization is critical for MtsR regulatory activity. Finally, the *mtsR* mutant strains defective in metal sensing and oligomerization are attenuated for virulence in a mouse model of invasive infection, indicating that Mn sensing and gene regulation by MtsR are critical processes during *S. pyogenes* infection.

INTRODUCTION

Manganese (Mn) is an essential nutrient for bacterial growth due to its role as a protein cofactor in cellular processes such as cell division, oxidative stress defenses and DNA synthesis and repair (1–6). Thus, pathogenic bacteria must acquire Mn during infection for successful survival in the host (7). Although Mn is beneficial for microbial growth, Mn in excess can be toxic to the bacteria (7). This necessary balance between metal sufficiency and metal toxicity is targeted by the host nutritional immune mechanisms, as the host employs metal starvation or metal poisoning to control microbial growth (2,8–13). As a countermeasure, pathogens employ Mn importers or exporters in response to alterations in extracellular Mn availability (2,14). A crucial component of the bacterial Mn homeostasis mechanism is the Mn-sensing transcription regulator that couples metal availability with regulation of the genes encoding Mn import and export systems (15–17). During metal sufficiency, these metalloregulators bind the cognate metal and repress the transcription of metal importers through association with target promoters. Conversely, when Mn limitation occurs, the metal-free transcription regulators dissociate from the promoter and relieve the repression of target gene expression (18,19). Despite the wealth of data on the biochemical and structural characterization of Mn-sensing bacterial transcription regulators (20–24), their contribution to bacterial virulence is poorly understood.

Group A *streptococcus* (GAS), also known as *Streptococcus pyogenes*, is a major human pathogen that causes a broad spectrum of diseases ranging from mild pharyngitis and impetigo to the life-threatening necrotizing fasciitis and streptococcal toxic shock syndrome (25,26). As for other pathogenic bacteria, GAS encounters host-imposed zinc (Zn) limitation during invasive infection (12). GAS colonization surfaces are enriched with neutrophil-derived extracellular metal binding protein, calprotectin (CP) (12). CP is a heterodimer of S100A8 and S100A9 proteins that is se-

*To whom correspondence should be addressed. Tel: +1 713 441 5252; Fax: +1 713 441 7295; Email: mkumaraswami@houstonmethodist.org

creted at the site of infection by neutrophils. Upon secretion, the extracellular CP sequesters Zn and Mn from bacterial colonization surfaces and inhibits microbial growth by metal starvation (9,10,27). To overcome CP-mediated Zn limitation, GAS monitors Zn availability through the Zn-sensing transcription regulator, AdcR, and outcompetes CP in Zn acquisition by upregulating the expression of high-affinity Zn importer, *adcABC* (12,28). However, analogous Mn sensing mechanisms and adaptive responses to Mn limitation in GAS remain poorly characterized.

To monitor metal stress conditions, GAS employs four metalloregulators: AdcR, GczA, MtsR, and PerR (13,28–30). With the exception of MtsR, the cognate ligand for the other metalloregulators has been identified. AdcR senses Zn limitation (28), whereas GczA monitors Zn surplus (13). The sensing of peroxide stress by PerR requires iron (Fe) (29). On the other hand, MtsR is proposed to be a dual metal-sensing regulator that mediates gene regulation in response to both Fe and Mn availability (30,31). Consequently, ambiguity exists regarding the identity of metal ligand sensed by MtsR.

GAS encodes four known ATP-binding cassette (ABC) family transporters for metal acquisition. The three-component transporter encoded by *adcABC* is involved in Zn uptake (12). Heme acquisition is carried out by the HtsABC transporter and shp/shr protein (32–35), and FtsABCD importer is implicated in ferric ferrichrome acquisition (36). However, conflicting evidence exists regarding the specific metal ligand transported by MtsABC and its contribution to GAS physiology. Structural and biochemical data indicate that the membrane-anchored lipoprotein, MtsA, binds Fe with high affinity (37,38). Consistent with this, inactivation of *mtsABC* resulted in reduced intracellular Fe and Zn levels, suggesting that MtsABC is an Fe or Zn importer (39). Another study showed that MtsABC transports both Mn and Fe, and contributes to GAS oxidative stress defenses (40). Consequently, GAS adaptive responses to Mn limitation and the role of MtsABC, or other yet to be identified metal transporters, in overcoming host-mediated Mn limitation remain poorly understood.

In this study, we show that MtsR is a Mn-sensing transcription regulator that upregulates genes encoding the Mn acquisition system (*mtsABC*), Mn-independent ribonucleotide reductase (*nrdEIF.2*), and putative iron or heme acquisition systems (*shr, shp* and *sia operon*) during Mn limitation. MtsR employs a complex regulatory mechanism to sense the severity of Mn deficiency and mount a measured regulatory response: a low-level upregulation of *mtsABC* controlled by the secondary metal-sensing site, site 2, and robust induction of *mtsABC* expression controlled by Mn sensing at the primary metal-sensing site, site 1. Finally, we report a previously unknown role for the C-terminal FeoA domain in MtsR oligomerization on target promoter sequences. Importantly, we demonstrate that FeoA domain-dependent MtsR multimerization is critical for its regulatory activity and contributes significantly to GAS virulence. Given that FeoA domains are present in most of the DtxR family regulators, we propose that FeoA domain-dependent oligomerization and gene regulation is a common allosteric strategy in DtxR family metalloregulators.

MATERIALS AND METHODS

Bacterial strains, plasmids and growth conditions

Bacterial strains and plasmids used in this study are listed in Supplementary Table S1. Strain MGAS10870 was used as the wild type GAS (WT) in this study. MGAS10870 is a previously described invasive serotype M3 isolate whose genome has been fully sequenced (41). MGAS10870 is representative of serotype M3 strains that cause invasive infections, and has WT sequences for all known major regulatory genes (41). *Escherichia coli* DH5α strain was used as the host for plasmid constructions and BL21(DE3) strain was used for recombinant protein overexpression. GAS was grown routinely on Trypticase Soy agar containing 5% sheep blood (BSA; Becton Dickinson) or in Todd-Hewitt broth containing 0.2% (w/v) yeast extract (THY; DIFCO). Chelexed THY was prepared by incubating the medium with chelex-100 beads (Sigma-Aldrich, USA), and the metal-depleted medium was subsequently supplemented with $CaCl_2$ (250 μM), $MgCl_2$ (1 mM) and $ZnSO_4$ (10 μM). The *Escherichia coli* strain used for protein overexpression was grown in Lysogeny broth (LB broth; Fisher). When required, kanamycin or spectinomycin was added to a final concentration of 50 μg/ml. Chloramphenicol was used at a final concentration of 15 μg/ml. All GAS growth experiments were done in triplicate on three separate occasions for a total of nine replicates. Overnight cultures were inoculated into fresh media to achieve an initial absorption at 600 nm (A_{600}) of 0.03. Bacterial growth was monitored by measuring the absorption at 600 nm (A_{600}).

Construction of *mtsR*-inactivated mutant strain

Insertional inactivation of the *mtsR* gene in WT GAS was performed by methods described previously (42–44). Briefly, a PCR fragment containing a spectinomycin resistance (*spc*) cassette with the fragment of gene to be deleted on either side was generated in a three-step PCR process. Subsequently, the plasmid with the spc gene disruption cassette was introduced into the parent strain by electroporation, and the gene was disrupted through homologous recombination. The isogenic mutant strains were selected by growth on spectinomycin-containing medium. Inactivation of the gene was confirmed by DNA sequencing. Primers used for the construction of the isogenic Δ*mtsR* mutant strain are listed in Supplementary Table S2.

Construction of *mtsR trans*-complementation plasmid

To complement the isogenic Δ*mtsR* mutant strain, the coding sequence of the full-length *mtsR* gene together with the *mtsR* promoter region was cloned into the *E. coli*-GAS shuttle vector *pDC123* (45). Using the primers listed in Supplementary Table S2, the fragment was cloned into *pDC123* and the insert was verified by DNA sequencing. The plasmid containing the *mtsR* gene and promoter was electroporated into the isogenic Δ*mtsR* mutant strain.

RNA sequencing (RNA-seq)

GAS strains were grown to mid-exponential phase of growth ($A_{600} \sim 1.0$) in THY broth. Subsequently, cells were

incubated for 30 min in the presence or absence of 100 μM $MnCl_2$. GAS has relatively higher mRNA turnover rate and the mean half-life of GAS mRNA is estimated to be 1.26 min (46). Thus, to minimize mRNA decay, we stacked the growth of individual strains or replicates 30 min apart, added the samples to RNAprotect in less than a minute, and harvested by centrifugation. RNA isolation and purification were performed using an RNeasy (Qiagen) mini kit according to the manufacturer's protocol and treated with DNase using the TURBO DNA-free kit (Ambion). RNA was analyzed for quality and concentration with an Agilent 2100 Bioanalyzer. The ribosomal RNA was then removed using a Ribo-Zero treatment kit (Epicenter) according to manufacturer's protocol and further purified using the Min-Elute RNA purification kit (Qiagen). The rRNA-depleted RNA was then used to synthesize adaptor-tagged cDNA libraries using the ScriptSeq V2 RNA-seq library preparation kit (Epicenter). cDNA libraries were then run on a NextSeq instrument using the Illumina v2 reagent kit (Illumina). Approximately 10 million reads were obtained per sample and the reads were mapped to the MGAS315 genome using the CLC-Genomics WorkBench, version 11 (CLC Bio). For RNA-seq analysis, the total number of reads per gene between the replicates was normalized by TPM [(transcripts/kilobase of gene)/(million reads aligning to the genome)]. Using the TPM values, pair-wise comparisons were carried out between the two strains to identify the differentially expressed genes. Genes with 2-fold difference and $P < 0.05$ after applying Bonferroni's correction were considered to be statistically significant.

MtsR overexpression and purification

The coding region of the full-length *mtsR* gene of strain MGAS10870 was cloned into plasmid pET-28a. Protein was overexpressed in *E. coli* strain BL21 (DE3). Cells were grown at 37°C until the A_{600} reached 0.5 and then were induced with 0.5 mM IPTG at 25°C overnight. Cell pellets were suspended in 50 ml of buffer A (20 mM Tris pH 8.0, 200 mM NaCl, 1 mM Tris 2-carboxyethyl phosphine hydrochloride (TCEP) and 30 mM imidazole) supplemented with one protease inhibitor cocktail pellet and DNase I to a final concentration of 5 μg/ml. Cells were lysed by a cell disruptor (Microfluidics) and cell debris was removed by centrifugation at 15 000 rpm for 30 min. The clarified cell lysate was loaded onto a pre-equilibrated Ni-NTA agarose column and bound MtsR was eluted using buffer A containing 300 mM imidazole. The concentrated MtsR was buffer exchanged into storage buffer (20 mM Tris pH 8.0, 200 mM NaCl, 1 mM TCEP and 5% v/v glycerol) by size exclusion chromatography with Superdex 200 G column. The protein was purified to > 95% homogeneity and concentrated to a final concentration of ∼8 mg/ml. To cleave the hexa-histidine tag, the purified MtsR was incubated with thrombin (5 units per mg of MtsR) (GE Healthcare) at 4°C. The untagged MtsR was further purified by Ni-NTA affinity chromatography and thrombin cleavage of the eluted untagged MtsR was verified by SDS-PAGE. Subsequently, MtsR was purified by size exclusion chromatography with Superdex 200 G column. The purified untagged MtsR was subjected to two rounds of overnight dialysis against storage buffer containing 10 mM EDTA to remove trace metals bound to the protein. Finally, MtsR was dialyzed against chelexed (chelex beads, Sigma) storage buffer to prepare the metal-free apo form of MtsR. The protein was concentrated to a final concentration of ∼8 mg/ml. The untagged protein was used for crystallographic studies and biochemical characterization of MtsR.

Electrophoretic mobility shift assay

Oligonucleotides containing the putative MtsR-binding site (*mts* motif) from the *mtsABC* promoter (5′ TTAATTAAGTTTAGTTAATTATCCCCCATAAT TAACTAAACTTAATTAA-3′) were annealed by heating at 95°C for 5 min followed by slow cooling to room temperature. Binding reactions were carried out in 20 μl volume of binding buffer (20 mM Tris pH 8.0, 200 mM NaCl, 1 mM TCEP and 5% v/v glycerol) containing 50 nM of oligoduplex and increasing concentrations of recombinant MtsR. After 15 min incubation at room temperature, the reaction mixtures were resolved on a 10% native polyacrylamide gel supplemented with 5% (v/v) glycerol for 100 min at 100 V at 4°C in Tris Borate buffer with 5% (v/v) glycerol. The gels were stained with ethidium bromide and analyzed on a BioRad Gel Electrophoresis Systems.

Fluorescence polarization assay

Fluorescence polarization-based MtsR-DNA binding experiments were performed with a Biotek microplate reader (Biotek) using the intrinsic fluorescence of fluorescein-labelled DNA. The polarization (P) of the labeled DNA increases as a function of protein binding, and equilibrium dissociation constants were determined from plots of millipolarization ($P \times 10^{-3}$) against protein concentration. For MtsR-DNA-binding studies, 1 nM 5′-fluoresceinated oligoduplex (5′ TTAATTAAGTTTAGTTAATTATCC CCCATAATTAACTAAACTTAATTAA-3′) in binding buffer (20 mM Tris pH 8.0, 200 mM NaCl, 1 mM Tris 2-carboxyethyl phosphine hydrochloride (TCEP) and 5% v/v glycerol) was titrated against increasing concentrations of purified MtsR and the resulting change in polarization was measured. Samples were excited at 490 nm and emission measured at 530 nm. All data were plotted using KaleidaGraph and the resulting plots were fitted with the equation $P = \{(P_{bound} - P_{free})[protein]/(K_D + [protein])\} + P_{free}$, where P is the polarization measured at a given protein concentration, P_{free} is the initial polarization of the free ligand, P_{bound} is the maximum polarization of specifically bound ligand and [protein] is the protein concentration. Non-linear least squares analysis was used to determine P_{bound}, and K_d. The binding constant reported is the average value from at least three independent experimental measurements.

To determine the binding stoichiometry of MtsR to the 22 bp *mts* motif, the binding condition identical to those used in the FP binding affinity determination experiments was used. However, to ensure stoichiometric binding, the concentration of the DNA site was increased to 20-fold above the K_d by using a mixture containing 1 nM 5′-fluoresceinated DNA and an amount of unlabeled DNA

necessary to achieve a concentration 20-fold above K_d. MtsR was titrated into the binding solution and the graph of the resulting data shows a linear increase in the observed mP until saturation with DNA, after which the mP values showed no steep increase. The binding stoichiometry for the DNA site was obtained from the MtsR concentration values at which inflection point occurs.

Transcript level analysis

GAS strains were grown to the indicated A_{600} and incubated with two volumes of RNAprotect (Qiagen) for 10 min at room temperature. RNA isolation and purification were performed with an RNeasy kit (Qiagen). After quality control analysis, cDNA was synthesized from the purified RNA using Superscript III (Invitrogen) and quantitative RT-PCR (qRT-PCR) was performed with an ABI 7500 Fast System (Applied Biosystems). Comparison of transcript levels was performed by the ΔC_T method of analysis using *tufA* as the endogenous control gene (28,47). The primers and probes used for qRT-PCR are listed in Supplementary Table S2.

Crystallization and structure determination of MtsR

To prepare the Mn-bound MtsR complex, apo MtsR was dialyzed against buffer containing 20 mM Tris pH 8.0, 200 mM NaCl, 1 mM TCEP, 5% v/v glycerol and 0.5 mM $MnCl_2$. After overnight dialysis at 4°C, the complex was dialyzed against unsupplemented chelexed buffer to eliminate excess Mn. The protein was concentrated to 7.5 mg/ml using an YM-10 Amicon concentrator (Millipore). Crystallization of MtsR was performed using the vapor diffusion method with the crystallization solution containing 40 mM sodium acetate, 0.16 M magnesium formate, 2.6 M lithium acetate, 20% (v/v) PEG 2000, 66 mM ammonium sulfate, and 0.8 mM manganese chloride. Preliminary crystals were further optimized for diffraction quality by adding benzamidine hydrochloride (2% v/v) as an additive to the crystallization solution. The diffraction data of the MtsR crystals were collected at the Advance Light Source (ALS) beam line 8.3.1 (Berkeley, CA, USA). Data were processed with iMOSFLM (48) and SCALA (49). Iterated rounds of model building were done using 'COOT' (50) and refinement of the built model was performed using Refmac5 and Phenix (51). The quality of the final model was verified using Molprobity (52,53). Selected X-ray data collection, phasing, and refinement statistics are given in Supplementary Table S3. All structure-related figures were generated using Pymol (54).

Site-directed mutagenesis of MtsR

Plasmid pET28a-*mtsR* or pDC-*mtsR* containing the WT *mtsR*-coding region was used as template for the site-directed mutagenesis. QuikChange site-directed mutagenesis kit (Stratagene) was used to introduce single amino acid substitutions within the *mtsR* coding region, and mutations were verified by DNA sequencing. The primers used to introduce the substitutions are listed in Supplementary Table S2.

Gel filtration chromatography

Size exclusion chromatography was used to determine the oligomerization states of recombinant WT and mutant derivatives of MtsR. A Superdex column (GE healthcare) was calibrated using cytochrome C (Mr 12 400), carbonic anhydrase (Mr 29 000), bovine serum albumin (Mr 66 000), alcohol dehydrogenase (Mr 150 000) and β-amylase (200 000). The $K_{Average}$ (K_{ave}) was calculated using the equation $K_{ave} = (V_E - V_O)/(V_T - V_O)$, where V_T, V_E and V_O are the total column volume, elution volume and void volume of the column respectively. A standard graph was obtained by plotting the logarithm of the molecular weight (Mr) versus the K_{ave} (Graphpad prism). The K_{ave} of each marker as well as the experimental samples were the average value of two or more experiments.

Metal content analysis by ICP-MS

The recombinant WT or mutant MtsR proteins were prepared for metal content analysis as described above. To determine the intracellular metal content, GAS strains were grown to mid-exponential phase, incubated with or without 100 μM $MnCl_2$ for 30 min, and cells were harvested by centrifugation. Cell pellets were washed once with chelexed phosphate-buffered saline (PBS) containing 1 mM nitrilotriacetic acid and twice with chelexed PBS, and cell pellets were stored at −80°C till use. Cells were resuspended in chelexed PBS, lysed by fast prep, and the total protein concentration in the clarified cell lysate was measured by Bradford assay. The metal content of purified protein preparations or cell lysates was determined using the ICP-MS DRCII system (PerkinElmer Life Sciences) with gallium as an internal standard as described previously (35). All the measurements were recorded in triplicates using 2% (v/v) ultra-pure nitric acid diluted samples from a 10 μM purified protein stock solution. The final average metal content is reported.

Mouse virulence studies

Mouse experiments were performed according to protocols approved by the Houston Methodist Research Institute Institutional Animal Care and Use Committee. These studies were carried out in strict accordance with the recommendations in the Guide for the Care and Use of Laboratory Animals, eighth edition. Virulence of the isogenic mutant GAS strains was assessed using intramuscular mouse model of infection (approved number AUP-0318-0016). For intramuscular infection, 10 female 3–4 week-old CD1 mice (Harlan Laboratories) were inoculated in the right hindlimb with 1×10^7 CFU of each strain and monitored for near mortality. Results were graphically displayed as a Kaplan-Meier survival curve and analyzed using the log-rank test.

Statistical analysis

Prism (GraphPad Software 7.0) was used for statistical analyses. All GAS growth experiments for transcript level analyses were done in triplicate on three separate occasions for a total of nine replicates. Statistical significance for transcript level analyses between samples was determined by *t*

test. The MtsR-DNA binding and MtsR-Mn experiments were done on three separate occasions to ensure reproducibility. For near mortality, values are shown as Kaplan–Meier survival curves, and statistical significance was determined using the log-rank test.

RESULTS

GAS adaptive responses to Mn limitation

To elucidate the molecular components of GAS adaptive responses to Mn limitation, we compared the transcriptome of wild-type (WT) GAS grown in Mn-replete and -deficient growth conditions by RNA sequencing (RNA-seq). GAS was grown in laboratory medium (THY) to mid-exponential growth phase ($A_{600} \sim 1.0$) and incubated with or without 100 μM $MnCl_2$ for 30 min. Unsupplemented THY was treated as the Mn deficient growth condition. GAS genes with ≥2-fold change in transcript levels between the two growth conditions with statistical significance ($P < 0.05$) were considered differentially regulated (Supplementary Tables S4 and S5). A total of 17 genes were differentially regulated, with 10 genes upregulated and 7 genes downregulated during Mn limitation. Genes encoding the putative tripartite ATP-binding cassette (ABC) family Mn importer, *mtsABC*, were highly upregulated during Mn limitation (Supplementary Table S4). Other upregulated genes of known function include the Fe acquisition system (*shr* and *fhuD.2*), Fe efflux pump (*pmtA*) and hemolytic CAMP factor, *cfa*, (Supplementary Table S4). Conversely, GAS genes downregulated during Mn limitation include hypothetical proteins of unknown function (Supplementary Table S5). These results indicate that upregulation of *mtsABC* constitutes the major GAS adaptive response to Mn limitation, suggesting a likely role for MtsABC-mediated Mn acquisition in overcoming metal deficiency.

GAS adaptive responses to Mn limitation is controlled by MtsR

The expression of *mtsABC* is controlled by the divergently transcribed regulator, MtsR (31,55). Three independent studies in two GAS *emm* serotypes (*emm3* and *emm49*) previously determined the regulon controlled by MtsR (55–57). However, the composition of *mtsR* regulon varied significantly between the two serotypes. In serotype M49 GAS, MtsR controls Fe and heme acquisition systems. However, no MtsR-dependent regulation of *mtsABC* was observed (57). In serotype M3 GAS, MtsR controls a much larger regulon that includes modest upregulation of *mtsABC* (55). In addition to possible serotype-specific differences in gene regulation by MtsR in the two genetically-distinct GAS serotypes, an underappreciated component in the transcriptome studies was the Mn concentration in the growth conditions used. The nutrient-rich laboratory medium (THY) contains only 250 nM Mn compared to micromolar concentrations of Zn and Fe (58). Thus, we hypothesized that during GAS growth in Mn-limited, unsupplemented THY, MtsR exists in a metal-free, inactive state, and is unable to mediate Mn-dependent gene regulation. To test this hypothesis, we constructed an insertionally-inactivated isogenic *mtsR* mutant strain in the parental serotype MGAS10870 (*ΔmtsR*) and compared *mtsA* transcript levels in the WT and *ΔmtsR* mutant strains by qRT-PCR. Consistent with our hypothesis, *mtsA* transcript levels in WT GAS grown in unsupplemented THY is comparable to that of *ΔmtsR* mutant strain (Supplementary Figure S1). However, supplementation of THY with Mn resulted in decreased *mtsA* transcript levels in WT GAS, and maximal repression of *mtsA* expression was observed in THY supplemented with 100 μM Mn (Supplementary Figure S1). Thus, comparisons of WT and *ΔmtsR* mutant strains in THY medium may not elucidate the precise Mn-specific regulon controlled by MtsR as MtsR is functionally inactive in WT grown in THY.

Thus, to determine the contribution of Mn-dependent gene regulation by MtsR to GAS adaptive responses to Mn limitation, we performed comparative transcription profiling of WT and *ΔmtsR* strains by RNA-seq under Mn replete conditions. GAS strains were grown in THY to mid-exponential growth phase ($A_{600} \sim 1.0$) and incubated with 100 μM $MnCl_2$ for 30 min. Three biological replicates were used for each strain. Transcript levels of GAS genes with ≥2-fold changes between the strains with statistical significance ($P < 0.05$) are summarized in Supplementary Tables S6 and S7. Compared to previous studies, MtsR controls a much smaller regulon under the growth conditions used in this study. A total of 26 genes were differentially regulated, with all the identified genes being downregulated by MtsR (Supplementary Tables S6 and S7). Major categories of genes controlled by MtsR include Mn (*mtsABC*) and Fe (*sia* operon, *SpyM3_1551–1561*) acquisition systems (Supplementary Figure S2). Furthermore, genes encoding metal-independent ribonucleotide reductase (*nrdF.2*, *nrdI.2* and *nrdE.2*) (Supplementary Figure S2), and Fe efflux transporter (*pmtA*) were also negatively regulated by MtsR. Collectively, the transcriptome studies elucidate the precise *mtsR* regulon and demonstrate that MtsR is a transcriptional repressor that controls GAS adaptive responses to Mn limitation.

Transcription regulation of *mtsABC* by MtsR is Mn-dependent

The promoter sequences of the *mtsABC* have a putative MtsR binding site (*mts* motif) upstream of the *mtsA* translation start site (Figure 1A). Thus, we investigated whether MtsR requires Mn to bind *mts* motif sequences by electrophoretic gel mobility shift assay (EMSA). First, we compared DNA binding by apo- and Mn-metallated MtsR. The apo MtsR failed to bind oligoduplexes containing the putative *mts* motif (Figure 1B). However, MtsR bound mts motif in the presence of Mn, and addition of the chelator EDTA disrupted MtsR-DNA interactions, indicating that MtsR requires Mn to bind DNA (Figure 1B). On the contrary, addition of Zn or Fe(III) resulted in smeared bands, indicating that MtsR engaged in weak and unstable interactions with *mts* motif in the presence of non-cognate metals (Figure 1B). Similarly, the Mn-metallated form of MtsR failed to bind non-cognate DNA, demonstrating that MtsR-DNA interactions are sequence-specific (Figure 1B). Together, these data indicate that MtsR-*mts* motif interactions are Mn-dependent and sequence-specific.

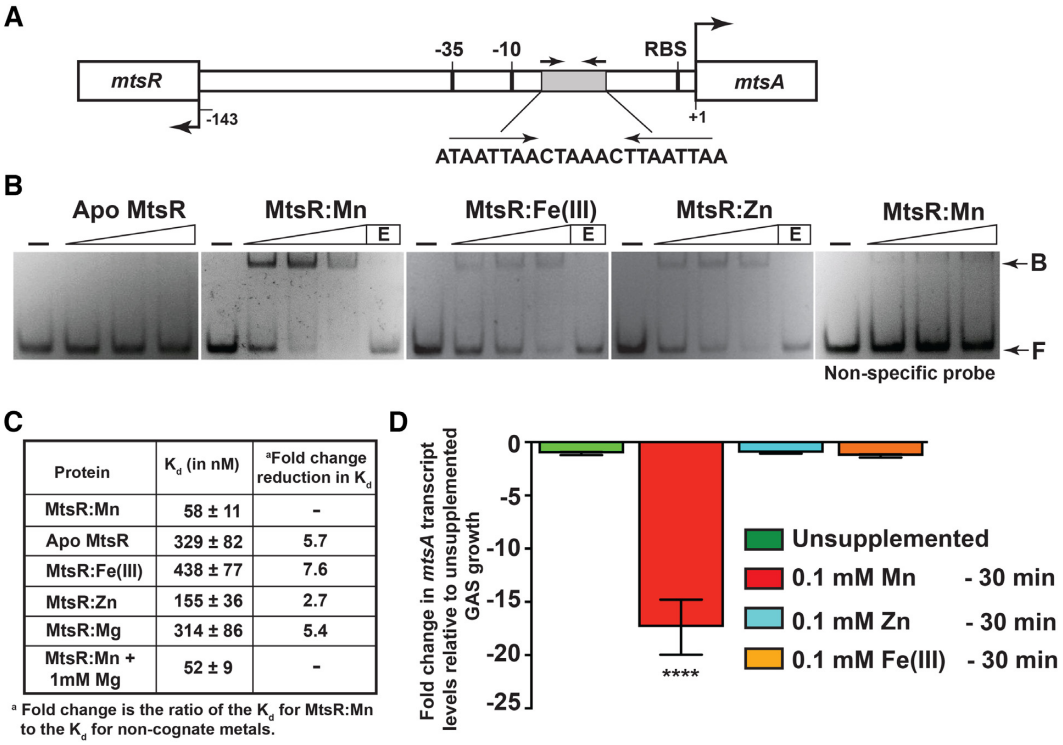

Figure 1. Transcription regulation of *mtsA* by MtsR is Mn dependent. (**A**) Genetic organization of the *mtsR* and *mtsA* gene region in GAS genome. The *mtsR* and *mtsA* genes are divergently transcribed. Numbers below the line indicate the nucleotide positions relative to the first nucleotide of the mtsA start codon. The putative –10 and –35 hexamers of the *mtsA* promoter and an inferred ribosomal-binding site (RBS) located upstream of *mtsA* labeled are marked and labeled above the line. The predicted MtsR-binding site in the *mtsA* promoter is marked by a shaded box and the pseudoinverted repeat within the MtsR-binding site is marked by arrows. The nucleotide sequence of the MtsR-binding site used in the electrophoretic mobility shift (EMSA) and fluorescent polarization (FP) analyses is shown. (**B**) The interactions between MtsR and the operator sequences in *mtsA* promoter as assessed by EMSA. Increasing concentrations (0, 100, 200 and 300 nM MtsR) of non-metallated (apo MtsR) or MtsR bound with different metals were incubated with oligoduplex containing the *mtsA* promoter sequences. The reaction mixtures were resolved on a 10% native-PAGE and the PAGE running buffer does not contain EDTA. Each indicated metal was added at a final concentration of 300 μM. The positions of free (F) and MtsR-bound (B) probes are labeled and indicated by arrows. E; indicates addition of metal chelator EDTA to the reaction mixture. (**C**) MtsR-*mts* motif binding constants assessed in the absence or presence of the indicated metals as assessed by fluorescent polarization (FP) assay. The apparent binding constants with standard deviations are shown. Each indicated metal was added at a final concentration of 10 μM and Mg was added at a final concentration of 1 mM. (**D**) Wild-type (WT) GAS was grown in THY medium to mid-exponential phase of growth (A_{600} 1.0) and incubated with 100 μM of the indicated metals for 30 min. Transcript level of *mtsA* was measured by qRT-PCR. Three biological replicates were performed and analyzed in triplicate. Data graphed are means ± standard deviation. Average values for unsupplemented samples were used as a reference and fold changes in transcript levels of the indicated samples relative to reference are shown. Statistical significance was determined by *t* test. **** indicates statistical significance with $P < 0.0001$ for the indicated samples compared to reference growth.

To better understand the effect of Mn on MtsR-DNA interactions, we performed fluorescence polarization (FP) assays with fluoresceinated oligoduplexes containing an *mts* motif in the presence or absence of $MnCl_2$ (Figure 1A). The MtsR:Mn complex bound to operator sequences with a dissociation constant (K_d) of 58 nM (Figure 1C and Supplementary Figure S3). However, when MtsR-DNA interactions were analyzed either in the absence of Mn (apo MtsR) or presence of non-cognate metals, a significant reduction in the affinity of MtsR for *mts* motif was observed (Figure 1C and Supplementary Figure S3). Addition of Zn resulted in slight reduction (2.7-fold increase in K_d) in the affinity. However, the lack of metal (5.7-fold increase in K_d) or inclusion of Fe(III) (7.6-fold increase in K_d) in the binding conditions drastically affected MtsR-DNA interactions (Figure 1C and Supplementary Figure S3). Since magnesium (Mg) is present in milli-molar concentrations in bacterial cytosol, we investigated the influence of Mg on MtsR–DNA interactions. The addition of Mg in the binding conditions did not alter the DNA binding properties of MtsR, suggesting that MtsR is selective for Mn (Figure 1C and Supplementary Figure S3). Together, these data demonstrate that high-affinity interactions between MtsR and *mtsA* promoter can be activated by Mn.

Next, we investigated whether the transcription regulation of *mtsA* by MtsR is Mn specific. GAS was grown to mid-exponential phase (A_{600} 1.0), exposed to 100 μM $MnCl_2$ for 30 min, and *mtsA* transcript level was measured by qRT-PCR. Consistent with our results from the DNA-binding studies, a 20-fold reduction in *mtsA* transcript levels was observed only in the presence of Mn compared to unsupplemented GAS growth (Figure 1D). Transcript levels of *mts*A in GAS grown in the presence of Zn and Fe were comparable to unsupplemented growth (Figure 1D), suggesting that MtsR-mediated repression of *mtsA* is Mn specific. Together, these results demonstrate that MtsR senses

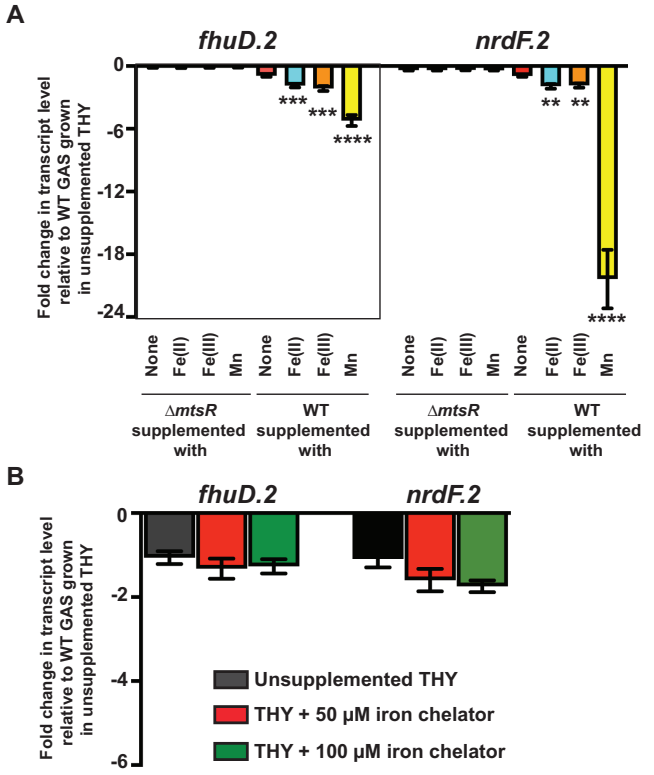

Figure 2. Transcription regulation of *fhuD.2* and *nrdF.2* by MtsR is Mn dependent. (**A**) Wild-type (WT) GAS or *ΔmtsR* mutant strain was grown in THY medium to mid-exponential phase of growth (A_{600} 1.0) and incubated with 100 μM of the indicated metals for 30 min. Transcript levels of *fhuD.2* and *nrdF.2* were measured by qRT-PCR. Three biological replicates were performed and analyzed in triplicate. Data graphed are means ± standard deviation. Average values for unsupplemented samples were used as a reference and fold changes in transcript levels of the indicated samples relative to reference are shown. (**B**) The WT GAS was grown in THY medium to mid-exponential phase of growth (A_{600} 1.0) and incubated with indicated concentrations of Fe chelator, 2, 2′-dipyridyl for 30 min. Transcript level of *fhuD.2* and *nrdF.2* were measured by qRT-PCR. Statistical significance was determined by *t* test. *P* values (**$P < 0.01$, ***$P < 0.001$, ****$P < 0.0001$) for the indicated samples compared to reference growth.

alterations in Mn availability and controls the expression of *mtsABC* by binding to the promoter.

MtsR-mediated gene regulation is Mn dependent

Previous studies indicated that MtsR is a dual regulatory protein that senses Mn and Fe, and controls the expression of iron acquisition systems (*sia* operon) in response to Fe availability. To investigate the Fe dependency of transcription regulation of *sia* operon and metal-independent ribonucleotide reductases (*nrdFIE.2*) (Supplementary Figure S2), we carried out two parallel investigations. First, we tested whether the addition of Fe or Mn to metal-depleted chelexed THY repressed the expression of *fhuD.2* and *nrdF.2* (Figure 2A). In parallel, we also assessed whether depletion of Fe from the growth medium by the addition of the Fe-specific chelator, 2,2′-dipyridyl, induced the expression of *fhuD.2* and *nrdF.2* (Figure 2B). Consistent with the results from RNA-seq experiments, inactivation of *mtsR* in the *ΔmtsR* mutant strain resulted in derepression of *fhuD.2* and *nrdF.2* genes (Figure 2A). The presence or absence of metals did not affect the regulatory outcome in the *ΔmtsR* mutant, indicating that MtsR controls the expression of *fhuD.2* and *nrdF.2* genes. Consistent with this, the promoters of *sia* operon and *nrdFIE.2* contain pseudopalindrome sequences similar to *mts* motif identified in *mtsA* promoter (Supplementary Figure S2). In WT GAS, the removal of Fe did not significantly affect the expression of *fhuD.2* and *nrdF.2* genes (Figure 2B). However, in the metal addition experiment, addition of Fe(II) or Fe(III) caused partial repression of *fhuD.2* and *nrdF.2* genes (Figure 2A). Contrarily, the addition of Mn caused a drastic reduction in *fhuD.2* and *nrdF.2* transcript levels compared to unsupplemented growth (Figure 2A), suggesting that transcription regulation of *fhuD.2* and *nrdF.2* is Mn-dependent. Together, these data indicate that MtsR-mediated transcription repression of the Fe acquisition machinery and metal-independent ribonucleotide reductases is strongly induced by Mn, whereas Fe only caused partial repression.

Structural basis for metal sensing by MtsR

To begin to elucidate the molecular basis for metal sensing and gene regulation by MtsR, we determined the crystal structure of MtsR to 3.1 Å resolution. The initial phases were determined by molecular replacement using the structure of Mn-sensing DtxR family metalloregulator SloR from *S. mutans* (PDB:5CVI) (23). Each asymmetric unit has two MtsR subunits. The structure has an overall topology of α1(5–18)-α2(23–31)-α3(35–47)-β1(51–54)-β2(57–61)-α4(63–87)-α5(93–104) α6(107–117)-β3(151–157)-α7(162–170)-β4(176–185)-β5(189–195)-β6(198–202)-α8(204–209)-β7(211–214) (Figure 3A). The MtsR subunit has the domain architecture characteristic of DtxR family regulators. Each subunit is composed of 3 domains: an amino-terminal DNA-binding domain (amino acids 1–62) containing a winged helix-turn-helix (wHTH) DNA binding motif, a central dimerization and metal binding domain (amino acids 63–137), and a carboxyl terminal FeoA-like domain (amino acids 138–215) (Figure 3A). Out of the two MtsR subunits in the asymmetric unit, only one subunit has well-defined electron density for the entire DNA-binding domain (Figure 3B). The flexible, less structured DNA-binding domain has been observed in the DNA-free structures of several transcription regulators (59). The three helices (α1-α3) of the N-terminal domain along with the two β-strands (β1–β2) form the characteristic wHTH motif in which helix α3 forms the 'recognition helix'. The recognition helix is predicted to make sequence-specific contacts in the major groove of its cognate DNA sequences, whereas the wing motif interacts with the bases in the adjacent minor grooves (60). The two subunits of MtsR are highly similar and their central and C-terminal domains can be superposed on to each other with a root mean square deviation (rmsd) of 0.61 Å.

As observed in other DtxR family metalloregulators, MtsR forms dimers in solution in the presence or absence of Mn (Supplementary Figure S4). An intermolecular interface similar to the dimer interface of other structurally characterized DtxR regulators was observed between the crystallographic symmetry-related molecules of MtsR (Figure

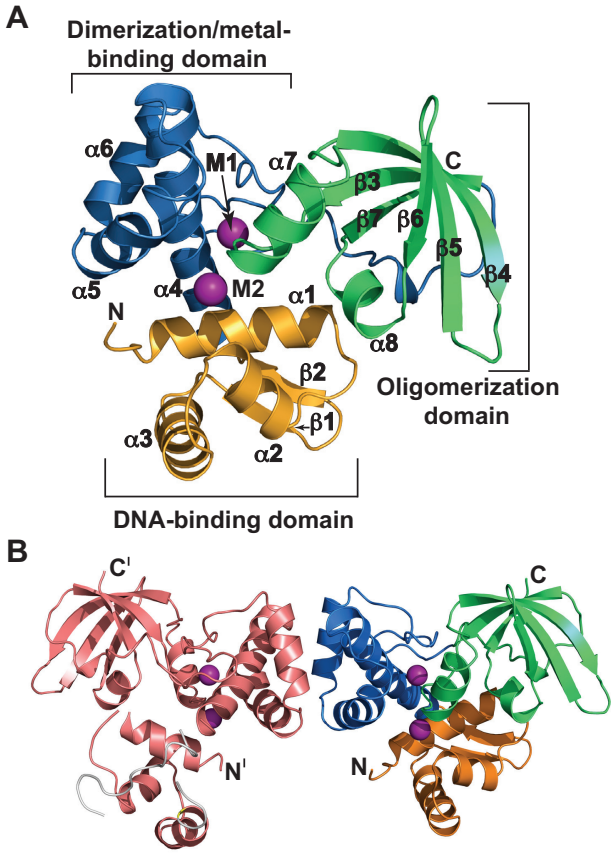

Figure 3. Crystal structure of MtsR. Ribbon representation of the crystal structure of an individual subunit (**A**) and dimeric form of MtsR (**B**). The three domains are labeled and color coded. The two metals bound to each MtsR subunit are shown as pink spheres and labeled M1 and M2. The secondary structural elements of MtsR subunit are labeled, and the amino- and carboxy-termini of the molecule are labeled as N and C, respectively. The first subunit of MtsR dimer is color coded as in panel A, whereas the second subunit is colored light pink. The amino- and carboxy-termini of the second subunit are labeled as N' and C', respectively.

3B and Supplementary Figure S5), which we designated as the MtsR dimerization interface. Solvent accessible surface area (SASA) analyses (61) revealed that a total of 778 Å^2 surface is buried in the dimer interface. The predominantly hydrophobic interactions among the amino acids F82 and L87 from helix α4, V100, L101 and V105 from helix α5, and F109 and I116 from helix α6 participate in MtsR dimerization.

Each MtsR subunit has two Mn atoms bound to the central dimerization domain (Figure 3). The metal at site 1 is coordinated by the side chains of amino acids H76 and E80 from helix α4, and C123 and H125 from the linker connecting the dimerization and FeoA domains (Figures 3 and 4A and B). The metal at site 2 is loosely bound and interacts with the side chains of H32 from helix α2, H95 from helix α5, and H161 and D163 from helix α8 (Figures 3 and 5A and B). Thus, the metal binding sites, site 1 and site 2, involve coordination by His-Glu-Cys-His and His-His-His-Asp motifs, respectively. The metals at both sites are in the interdomain region of MtsR among the dimerization, C-terminal, and DNA-binding domains. Thus, the metal occupancy at the two sites is ideally located to couple metal sensing with metal-dependent DNA binding and gene regulation by MtsR. Collectively, the crystal structure of MtsR revealed several structural elements that may be critical for gene regulation by MtsR.

MtsR dimerization is crucial for gene regulation

To determine the significance of the hydrophobic dimer interface to gene regulation by MtsR, we introduced single amino acid substitutions at two key hydrophobic residues in the dimerization domain, F82 and F109, with a charged glutamate residue (Supplementary Figure S5A and B). Introduction of charged residues in an apolar environment can be disruptive to the hydrophobic interactions and affect protein solubility. Thus, we hypothesized that glutamate substitutions in the dimer interface influence regulatory activity by altering the solubility of MtsR. To test this hypothesis, we compared the solubility of the overexpressed recombinant WT or mutant MtsR proteins by SDS-PAGE. Overexpression of the F82E and F109E mutant proteins was similar to WT MtsR (Supplementary Figure S5C). However, compared to WT MtsR, the recombinant mutant proteins, F82E and F109E, were predominantly present in the insoluble pellet fraction of the cell lysates (Supplementary Figure S5C), suggesting that the hydrophobic dimer interface is intolerant to substitutions with charged amino acids. The defective solubility hampered our ability to obtain F82E and F109E mutant proteins in sufficient quantity and purity to perform biochemical characterization. To test the biological significance of the dimer interface, we *trans*-complemented the *ΔmtsR* mutant strain with WT *mtsR* or variants containing single glutamate substitutions at F82 or F109 of MtsR and assessed the mutant strains for their ability to mediate Mn-dependent repression of *mtsA* transcription. Although the intracellular solubility of the WT and mutant MtsR proteins is unknown, the introduction of glutamate at either F82 or F109 of the dimerization domain resulted in the loss of Mn-dependent *mtsABC* repression by MtsR (Supplementary Figure S5D). The *mtsA* transcript levels in the mutant strains were comparable to that of the *ΔmtsR* mutant (Supplementary Figure S5D). Collectively, these results demonstrate that the hydrophobic interactions in the inter-subunit interface participate in MtsR dimerization and are critical for MtsR regulatory activity.

Metal binding site 1 is the primary Mn sensing site of MtsR

To investigate the contribution of Mn binding site 1 to metal sensing and metal-dependent gene regulation by MtsR, we introduced single alanine substitutions at site 1 metal ligands H76 and E80 (Figure 4A and B). The WT and mutant MtsR proteins were overexpressed and purified under metal-free conditions. The recombinant mutant MtsR proteins had WT-like protein solubility and formed WT-like dimers (Supplementary Figure S6), indicating that alanine substitutions did not induce protein misfolding or detrimentally affect MtsR dimerization. To test whether the single alanine substitutions at site 1 metal ligands affect Mn binding, we measured the Mn content of purified WT and mutant MtsR proteins by ICP-MS. The metal-free form of

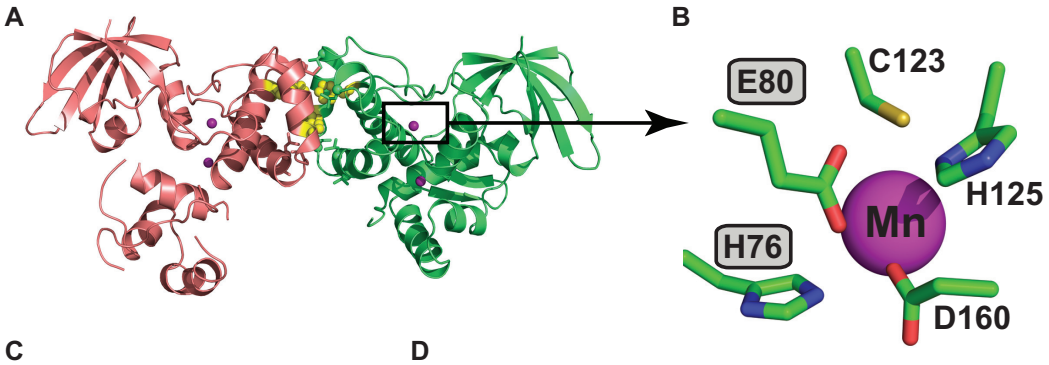

C

Protein	Mol of Mn per mol of MtsR[a]
Wild type MtsR	1.84 ± 0.13
MtsR-H76A	0.67 ± 0.05
MtsR-E80A	1.06 ± 0.07

[a] - Measurements were reported as average from triplicate studies

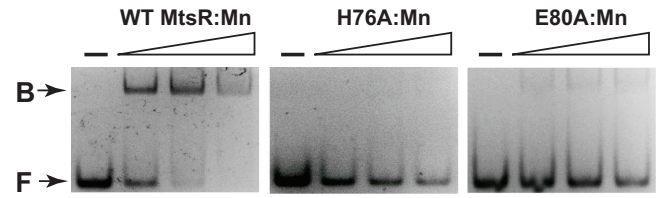

E

Protein	K_d (in nM)	[a]Fold change reduction in K_d
WT MtsR:Mn	58 ± 11	-
H76A:Mn	1400 ± 10	24
E80A:Mn	215 ± 60	3.7

[a] Fold change is the ratio of the K_d for WT MtsR:Mn to the K_d for mutant MtsR proteins.

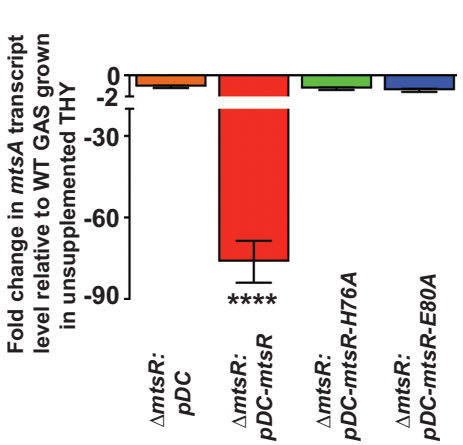

Figure 4. Characterization of isogenic *mtsR* mutant strains containing single alanine substitutions in site 1 Mn binding residues. (**A**) Ribbon representation of the MtsR dimer with the metal binding site 1 (boxed). The individual subunits of MtsR dimer are color coded. The metals bound to site 1 and site 2 in MtsR structure are shown as spheres and colored pink. (**B**) Magnified view of the Mn binding site 1. The side chains of the Mn-coordinating amino acids of site 1 are shown and labeled. The Mn-coordinating amino acids subjected to mutational analyses are highlighted in a shaded box. (**C**) Metal content analysis of recombinant WT or mutant MtsR proteins as determined by ICP-MS. (**D**) The interactions between recombinant WT or mutant MtsR and the operator sequences in *mtsA* promoter as assessed by EMSA. Increasing concentrations of WT or mutant MtsR (0, 100, 200 and 300 nM MtsR) proteins were incubated with oligoduplex containing the *mts* motif from *mtsA* promoter sequences and reaction mixtures were resolved on a 10% native-PAGE. Mn was added to a final concentration of 300 μM. The positions of free (F) and MtsR-bound (B) probes are labeled and indicated by arrows. (**E**) MtsR-*mts* motif binding constants for recombinant MtsR mutant proteins containing single alanine replacements in site 1 metal-contacting amino acid residues as assessed by FP assay. Mn was included at a final concentration of 10 μM. The apparent binding constants with standard deviations are shown. (**F**) GAS strains were grown in THY to the mid-exponential phase of growth, incubated with 100 μM $MnCl_2$ for 30 min, and *mtsA* transcript levels were measured by qRT-PCR. Three biological replicates were performed and analyzed in triplicate. Data graphed are means ± standard deviation. Average values for unsupplemented samples were used as a reference and fold changes in transcript levels of the indicated samples relative to reference are shown. Statistical significance was determined by *t* test. *P* values (****$P < 0.0001$) for the indicated strains were determined by comparison to the *ΔmtsR* mutant strain.

WT and mutant MtsR proteins were reconstituted to the Mn-bound form by dialyzing twice against chelexed buffer containing 50 μM $MnCl_2$ and once in chelexed buffer without Mn. Consistent with the structural observations, WT MtsR had close to two Mn atoms per subunit (4 Mn atoms in a dimer) (Figure 4C). Compared to WT MtsR, single alanine substitutions at H76 and E80 resulted in impaired Mn binding (Figure 4C), indicating that the site 1 metal ligands participate in Mn binding. Given that Mn is a corepressor required for DNA binding by MtsR, we next compared the DNA-binding properties of metallated forms of WT and mutant MtsR proteins by EMSA and FP. Compared to WT MtsR, no defined shifted bands were observed with H76A and E80A mutant proteins, indicating that both mutant proteins were defective in DNA binding (Figure 4D). Consistent with this, the affinity of the H76A

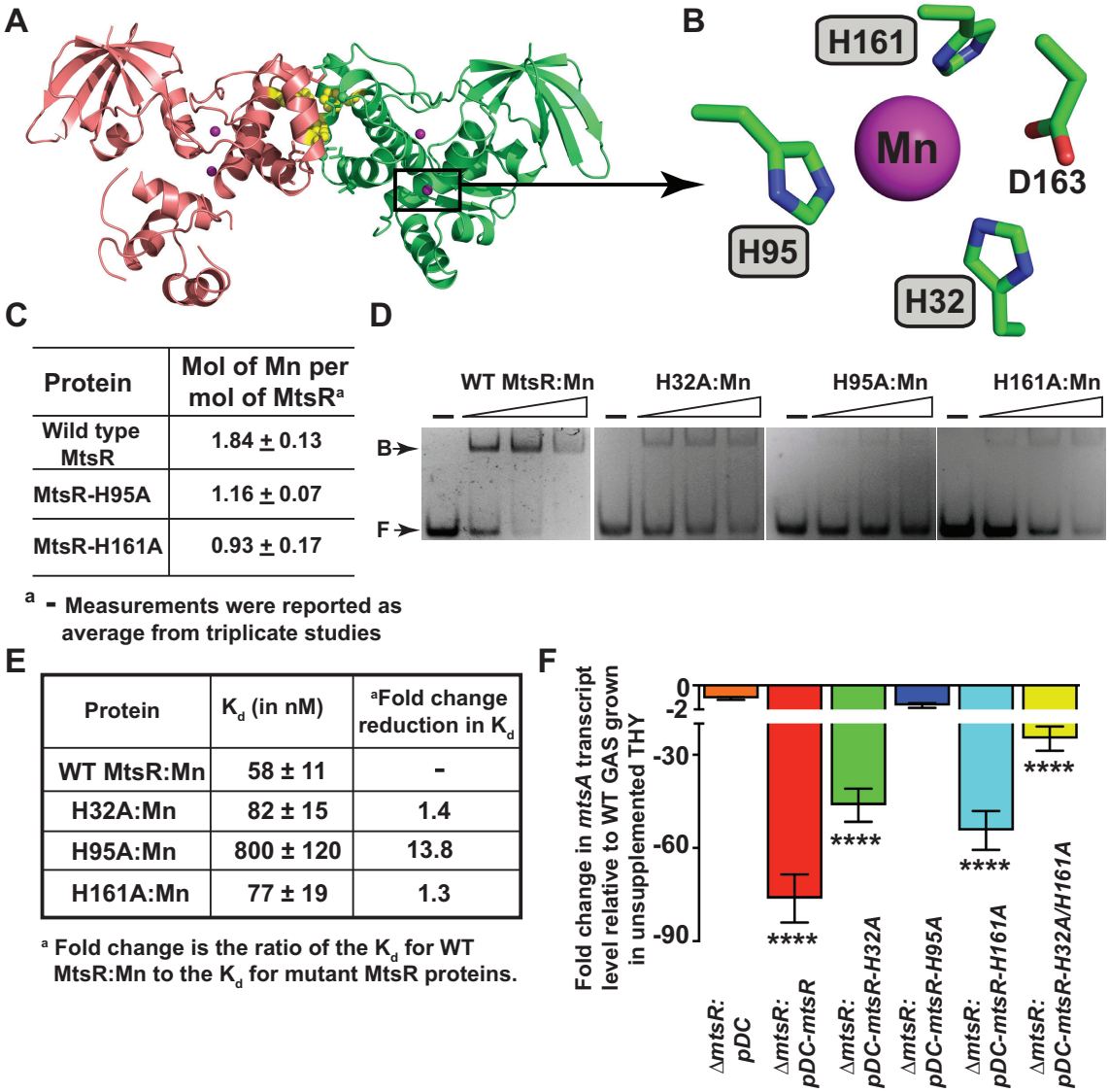

Protein	Mol of Mn per mol of MtsR[a]
Wild type MtsR	1.84 ± 0.13
MtsR-H95A	1.16 ± 0.07
MtsR-H161A	0.93 ± 0.17

[a] - Measurements were reported as average from triplicate studies

Protein	K_d (in nM)	[a]Fold change reduction in K_d
WT MtsR:Mn	58 ± 11	-
H32A:Mn	82 ± 15	1.4
H95A:Mn	800 ± 120	13.8
H161A:Mn	77 ± 19	1.3

[a] Fold change is the ratio of the K_d for WT MtsR:Mn to the K_d for mutant MtsR proteins.

Figure 5. Characterization of isogenic *mtsR* mutant strains containing single alanine substitutions in site 2 Mn binding residues. (**A**) Ribbon representation of the MtsR dimer with the metal binding site 2 (boxed). The individual subunits of MtsR dimer are color coded. The metals bound to site 1 and site 2 in MtsR structure are shown as spheres and colored in pink. (**B**) Magnified view of the Mn binding site 2. The side chains of the Mn-coordinating amino acids of the site 2 are shown and labeled. The Mn-coordinating amino acids subjected to mutational analyses are highlighted in a shaded box. (**C**) Metal content analysis of recombinant WT or mutant MtsR proteins as determined by ICP-MS. (**D**) The interactions between recombinant WT or mutant MtsR and the operator sequences in *mtsA* promoter as assessed by EMSA. Increasing concentrations of WT or mutant MtsR (0, 100, 200 and 300 nM MtsR) proteins were incubated with oligoduplex containing the *mts* motif from *mtsA* promoter sequences and reaction mixtures were resolved on a 10% native-PAGE. Mn was added to a final concentration of 300 μM. The positions of free (F) and MtsR-bound (B) probes are labeled and indicated by arrows. (**E**) MtsR-*mts* motif binding constants for recombinant MtsR mutant proteins containing single alanine replacements in site 2 metal-contacting amino acid residues as assessed by FP assay. Mn was included at a final concentration of 10 μM. The apparent binding constants with standard deviations are shown. (**F**) GAS strains were grown in THY to the mid-exponential phase of growth, incubated with 100 μM $MnCl_2$ for 30 min, and *mtsA* transcript levels were measured by qRT-PCR. Three biological replicates were performed and analyzed in triplicate. Data graphed are means ± standard deviation. Average values for unsupplemented samples were used as a reference and fold changes in transcript levels of the indicated samples relative to reference are shown. Statistical significance was determined by *t* test. *P* values (****$P < 0.0001$) for the indicated strains were determined by comparison to the *ΔmtsR* mutant strain.

and E80A mutant proteins for the *mts* motif was drastically decreased compared to WT MtsR (Figure 4E and Supplementary Figure S7). Finally, to assess the physiological relevance of metal occupancy at site 1 to gene regulation by MtsR, we compared *mtsA* transcript levels in WT and mutant strains grown in THY supplemented with Mn. The *mtsR-H76A* and *mtsR-E80A* mutant strains were unresponsive to Mn and the *mtsA* transcript levels in the mutant strains were comparable to that of the Δ*mtsR* mutant (Figure 4F), indicating that metal binding at site 1 is critical for Mn-dependent gene regulation by MtsR. Together, these data demonstrate that the metal binding site 1 is the primary Mn sensing site of MtsR and Mn occupancy at site 1 is crucial for metal-dependent repression of *mtsA*.

Metal binding site 2 participates in gene regulation by MtsR

To investigate the regulatory role of metal binding site 2 of MtsR, we introduced single alanine substitutions at three site 2 metal ligands: H32, H95, and H161 (Figure 5A and B). We have also generated double alanine substitutions at H32 and H161 (H32A/H161A). No alterations in protein solubility or dimerization were observed for the recombinant mutant proteins compared to WT MtsR (Supplementary Figure S6). When assessed for Mn binding by ICP-MS, the site 2 mutant proteins had decreased metal content compared to WT MtsR (Figure 5C), suggesting that the site 2 metal ligands are involved in Mn binding. To test the contribution of Mn occupancy at site 2 to DNA binding by MtsR, we assessed MtsR-DNA interactions by EMSA and FP. The smeary, labile complexes of H32A and H161A mutant proteins with DNA suggest that H32A and H161A mutant proteins were slightly defective in DNA binding compared to WT MtsR (Figure 5D). However, the lack of disappearance of free DNA in the presence of H95A mutant protein indicate that the DNA binding ability of the H95A mutant protein was drastically affected (Figure 5D). Consistent with the EMSA results, the affinity of H95A mutant to *mts* motif was decreased by 15-fold compared to WT MtsR (Figure 5E and Supplementary Figure S7). However, unlike the EMSA results, the H32A and H161A mutant proteins had affinities for *mts* motif that are comparable to WT MtsR (Figure 5E and Supplementary Figure S7).

Next, to investigate the regulatory influence of site 2 metal ligands on MtsR-dependent *mtsA* gene regulation, we compared the *mtsA* transcript levels in WT and isogenic *mtsR* mutant strains containing single or double alanine substitutions at site 2 metal ligands. The regulatory phenotype of the *mtsR* mutant strains was consistent with the DNA binding properties of MtsR. The *trans*-complemented strain (Δ*mtsR:pDC-mtsR)* had a 77-fold reduction in *mtsA* transcript levels relative to the *ΔmtsR* mutant (Figure 5F). However, the mutant strains containing alanine substitutions at site 2 metal ligands failed to mediate full repression of *mtsA*. The isogenic *mtsR-H95A* mutant strain had *mtsA* transcript levels similar to the *ΔmtsR* mutant strain (Figure 5F), suggesting that H95 of site 2 is crucial for gene regulation. Conversely, the *mtsR-H32A* (46-fold reduction in *mtsA* levels) or *mtsR-H161A* (54-fold reduction in *mtsA* levels) mutant strains displayed only partial repression of *mtsA* transcription. Furthermore, the *mtsR-H32A/H161A* double mutant (24-fold reduction in *mtsA* levels) strain was more defective in *mtsA* repression than the H32A or H161A mutant strains (Figure 5F). To explain the greater significance of H95 compared to other metal ligands of site 2, we took a closer look at the structural elements in the immediate vicinity of site 2. Among the site 2 metal binding ligands, only H95 is located in the immediate vicinity of primary metal sensing site 1. The amino acid H95 is located on helix α5, whereas the site 1 metal ligands H76 and E80 are located on helix α4 (Supplementary Figure S8A). Interestingly, extensive hydrophobic interactions were observed between the side chains of I79 and L83 of helix α4, and V94, A98 and L101 of helix α5 (Supplementary Figure S8B). Thus, alanine substitutions at H95 and the resulting defective metal binding at site 2 may affect the high affinity metal binding at site 1 indirectly and cause more defective gene regulation than other site 2 mutants. Therefore, it is possible that the regulatory phenotype of H95A is due to its collective participation in direct metal binding at site 2 and indirect influence on metal binding at site 1. Collectively, these results demonstrate that the Mn sensing site 2 participate in metal binding and gene regulation by MtsR. However, the site 2 has a lesser regulatory role than the primary Mn sensing site 1 of MtsR. Thus, we designate site 2 as the secondary Mn sensing site of MtsR.

Oligomerization of MtsR is critical for gene regulation

Most of the structurally characterized DtxR family metalloregulators have a C-terminal FeoA domain (20,21,23,24,62). However, the contribution of the C-terminal domain to the metal-dependent transcription regulation by DtxR family regulators remains unknown. In the crystal structure of MtsR, the C-terminal FeoA domain of one dimer is engaged in tail-to-tail interactions with the FeoA domain of the second dimer to form MtsR oligomer (Figure 6A). The oligomerization interface between two dimers is distinct from the MtsR dimerization interactions. A total surface area of 600 $Å^2$ is buried in the dimer-dimer interface (Figure 6A and B). These observations led us to hypothesize that the FeoA domain is involved in MtsR oligomerization and multimerization of MtsR is important for its gene regulatory activity. The oligomerization interface of MtsR is characterized by stacking interactions between the side chains of aromatic amino acids Y167 from helix α7 and F187 from the linker connecting strands β4 and β5 with the analogous amino acids from the second dimer (Figure 6B). To determine the biological relevance of the oligomerization interface in the FeoA domain to gene regulation by MtsR, we introduced single (F187A) or double (Y167A/F187A) alanine substitutions in MtsR. The alanine substitutions did not affect recombinant MtsR solubility or GAS viability (Supplementary Figure S6). The recombinant F187A or Y167A/F187A mutant proteins formed stable dimers in solution (Supplementary Figure S6B), indicating that the oligomerization interface does not participate in MtsR dimerization.

To assess the role of oligomerization interactions in the regulatory activity of MtsR, we assessed *mtsA* transcript levels by qRT-PCR in the isogenic mutant strains containing single or double alanine substitutions at the aromatic amino acids involved in MtsR oligomerization. Consistent with our hypothesis, the introduction of single or double alanine substitutions in the oligomeric interface resulted in loss of Mn-dependent repression of *mtsABC* by MtsR (Figure 6C), indicating that the FeoA domain is important for gene regulation by MtsR.

To elucidate the molecular basis for the interplay between MtsR oligomerization and gene regulation, we next tested the interactions between oligoduplexes containing MtsR binding site and recombinant MtsR mutant proteins by EMSA. The single alanine substitution (F187A) in the oligomerization domain of MtsR did not affect DNA binding (Figure 6D). Although the Y167A/F187A mutant protein was slightly defective in MtsR-DNA interactions compared to WT MtsR (Figure 6D), the DNA-binding abil-

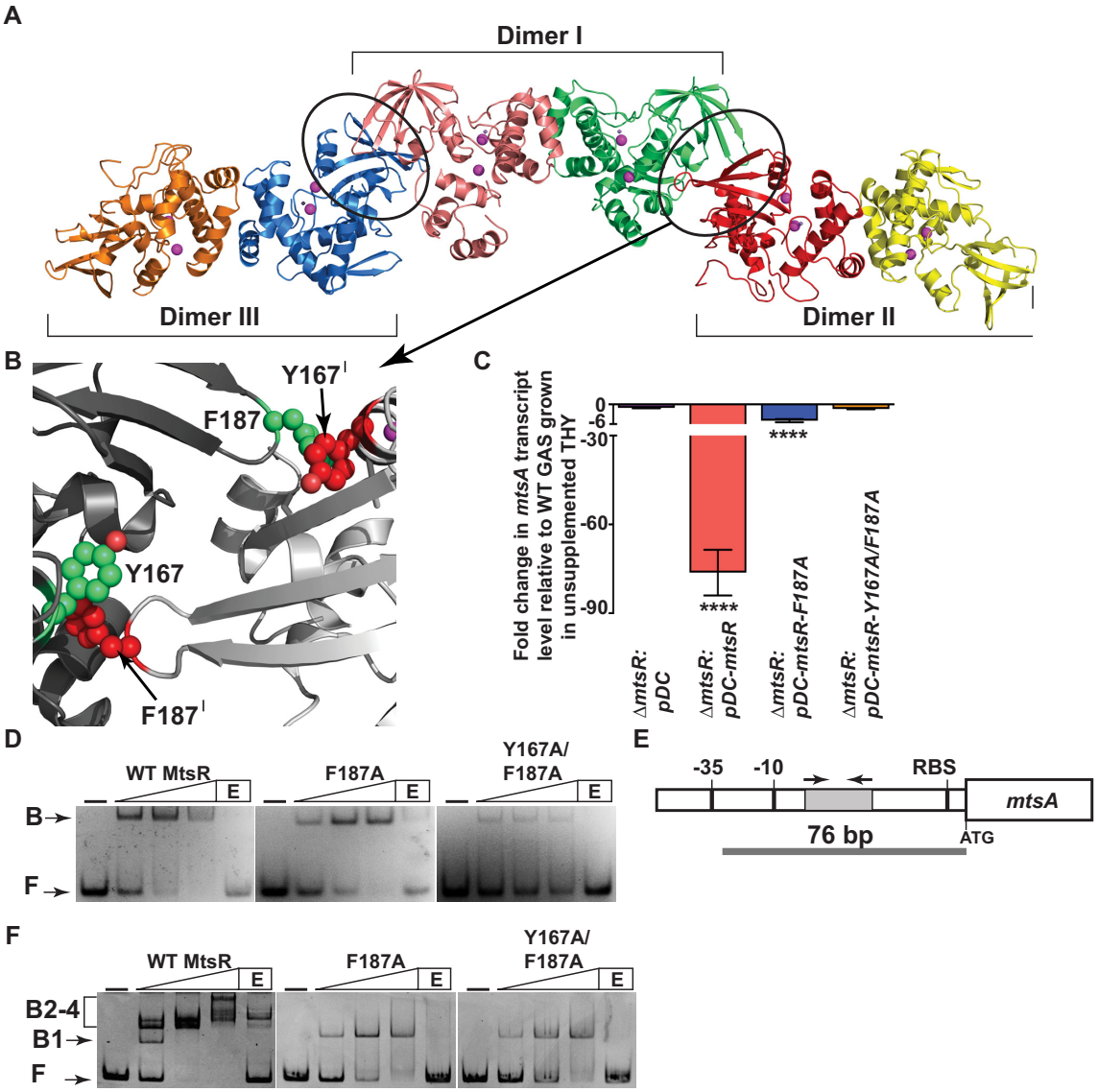

Figure 6. Oligomerization interface in the FeoA domain is involved in MtsR oligomerization on the promoter sequences and critical for Mn-dependent gene regulation. (**A**) Ribbon representation of crystallographic MtsR oligomer. Each subunit of MtsR is color coded and Mn bound to MtsR are shown as pink spheres. Three MtsR dimer molecules are shown and each dimer molecule is marked and labeled (Dimer I-III). The oligomerization interfaces in the FeoA domains of MtsR dimers are circled. (**B**) A magnified view of the intermolecular interactions at the FeoA domain of MtsR dimer in the circled area in panel A. The side chains of Y167 and Y187 located at the FeoA domain for two adjacent MtsR dimers are shown as sticks. The side chains from two dimers are color coded in green and red, respectively. The amino acid residues from the second dimer of MtsR dimer are indicated by Y167' and Y187'. (**C**) GAS strains were grown in THY to the mid-exponential phase of growth, incubated with 100 μM $MnCl_2$ for 30 min, and *mtsA* transcript levels were measured by qRT-PCR. Three biological replicates were performed and analyzed in triplicate. Data graphed are means ± standard deviation. Average values for unsupplemented samples were used as a reference and fold changes in transcript levels of the indicated samples relative to reference are shown. Statistical significance was determined by *t* test. *P* values (****$P < 0.0001$) for the indicated strains were determined by comparison to the *ΔmtsR* mutant strain. (**D**) The interactions between MtsR and the operator sequences in *mtsA* promoter as assessed by EMSA. Increasing concentrations of WT or mutant MtsR were incubated with oligoduplex containing the *mts* motif from *mtsA* promoter sequences and reaction mixtures were resolved on a 10% native-PAGE. Mn was added to a final concentration of 300 μM. The positions of free (F) and MtsR-bound (B) probes are labeled and indicated by arrows. (**E**) The schematics of the longer probe containing the MtsR-binding site and flanking sequences used in the electrophoretic mobility shift (EMSA) is shown. The mtsA gene is shown as a box and labeled. The putative -10 and -35 hexamers of the *mtsA* promoter and an inferred ribosomal-binding site (RBS) located upstream of mtsA labeled are marked and labeled above the line. The *mts* motif in the *mtsA* promoter is marked by a shaded box and the pseudo-inverted repeat within the MtsR-binding site is marked by arrows. The 76-bp DNA fragment corresponding to the longer probe used in the EMSA assay is shown as a grey box below the line. (**F**) The interactions between MtsR and probe containing the entire *mtsA* promoter sequences were assessed by EMSA. Increasing concentrations of WT or mutant MtsR proteins (0, 100, 200 and 300 nM MtsR) were incubated with longer probe containing the *mtsA* promoter sequences and reaction mixtures were resolved on a 10% native-PAGE. Mn was added to a final concentration of 300 μM. The positions of free (F) and MtsR-bound (B1–4) probes are labeled and indicated by arrows.

ity of MtsR mutant proteins failed to fully explain the defective gene regulation. Thus, we hypothesized that multimerization of MtsR on longer promoter sequences containing MtsR binding site and flanking sequences is critical for its gene regulatory activity. To test this hypothesis, we performed EMSA assays using a longer DNA probe containing the entire *mtsA* promoter (Figure 1A). Consistent with our hypothesis, the WT MtsR binds to the promoter sequences and forms multimeric MtsR-DNA complexes in a concentration-dependent manner (Figure 6E). Contrarily, the single and double alanine mutant proteins form a fast migrating MtsR-DNA complex and failed to form WT-like higher-order oligomeric MtsR–DNA interactions even at maximal protein concentration (Figure 6E). Collectively, these data indicate that the oligomerization interactions in the C-terminal FeoA domain promote MtsR multimerization on the *mtsABC* promoter and contribute to Mn-dependent gene regulation by MtsR.

To better understand the mode of MtsR multimerization on promoter sequences, we compared the DNA-binding properties of MtsR with the DNA-bound structures of Fe-sensing DtxR regulators. Structurally, DtxR from *Corynebacterium diphtheriae* and IdeR from *M. tuberculosis* bound to DNA duplex containing a single binding site as a dimer of dimers (63,64). The two dimers interact with the opposite sides of DNA duplex without any dimer to dimer interactions. Consequently, the DNA-bound conformation of the structurally characterized DtxR regulators is devoid of the oligomerization interactions observed in the crystal structure of MtsR, suggesting that MtsR-DNA interactions may be distinct from its structural homologs. Thus, to determine the stoichiometry between MtsR and DNA, we carried out a FP-based stoichiometry assay (59,65). The DNA binding site was added in 20-fold molar excess of the measured K_d and polarization was measured at each MtsR dimer titration point. The inflection point of the resulting curve at which all high-affinity specific sites are occupied by MtsR dimer concentration was used to deduce the stoichiometry. Results from the binding experiments using the 22-bp oligonucleotide duplex containing a *mts* motif showed that the inflection point occurs at 1 μM MtsR dimer in the binding reaction containing 1 μM DNA (Figure 7A). These results suggest that MtsR binds to 22-bp *mts* motif as a dimer, which is distinct from the DNA-binding mode of structurally characterized DtxR regulators. Nevertheless, consistent with our structural and biochemical findings, other studies also showed that MtsR multimerizes on the target promoter sequences. Depending on the promoter, MtsR interacts with large DNA fragments ranging from 42 to 130 bp and forms three or more higher order oligomers of unknown stoichiometry (31,57). To deduce the mode of MtsR multimerization on DNA, we docked DNA fragment manually to a preformed MtsR multimer that has three dimers (Figure 6A). Results from these analyses suggest that docking of 3 MtsR dimers may require a 70 bp DNA fragment and it is likely that significant deformation of DNA is required to accommodate the preformed MtsR multimer (Figure 7B). In this mode of DNA binding, MtsR dimers are spiraling along the DNA axis and adjacent MtsR dimers are related to each other by a 90° rotation on DNA (Figure 7B). The mode of MtsR multimerization suggested by our modeling studies is contrary to the DNA-bound structures of DtxR regulators in which adjacent dimers are related to each other by a 180° rotation on DNA axis and devoid of dimer to dimer interactions (63,64). Additional structural and biochemical investigations are required to validate the DNA-binding mode of MtsR multimers suggested by the modeling studies.

Mn-dependent gene regulation by MtsR is critical for GAS Virulence

To test the hypothesis that Mn binding ligands and oligomerization domain of MtsR are critical for *in vivo* Mn sensing, and GAS virulence, we performed animal infection studies using an intramuscular mouse model of infection. The WT GAS *trans*-complemented with empty vector *pDC123* was used as wild type (WT:*pDC*), and the isogenic Δ*mtsR* mutant *trans*-complemented with empty vector (Δ*mtsR:pDC*) was used as a negative control. We assessed the virulence phenotype of metal-binding site 1 mutants, *mtsR-H76A* and *mtsR-E80A*, and the double alanine mutant of the oligomerization domain, *mtsR-Y167A/F187A*. Mice were infected intramuscularly and monitored for near mortality for 7 days post-infection. Based on the virulence phenotype, the strains can be categorized into two groups as follows: the WT and *trans*-complemented strain (Δ*mtsR:pDC-mtsR*) had increased virulence relative to either the isogenic Δ*mtsR* mutant (Δ*mtsR:pDC*) or any of the tested mutant strains ($P < 0.05$ when comparing any two strains in different groups) (Figure 8A). There was no significant difference in mortality among strains within either of the two groups (Figure 8A). Together, these data indicate that Mn sensing and oligomerization function of MtsR are critical for GAS virulence.

To explain the attenuated virulence phenotype of the Δ*mtsR* mutant, we hypothesized that the dysregulation of *mtsABC* in the *ΔmtsR* mutant results in increased intracellular Mn accumulation, increased sensitivity to Mn intoxication, and reduced bacterial survival. To test this hypothesis, GAS strains were grown to mid-exponential phase of growth (A_{600} 1.0) and incubated in THY supplemented with or without additional 100 μM $MnCl_2$ for 30 min. The intracellular metal concentration of WT, *ΔmtsR* mutant, and the *trans*-complemented (Δ*mtsR:pDC-mtsR*) strains was measured by ICP-MS. The cytosolic concentrations of Fe, Mn, and Zn were similar in all 3 strains grown in unsupplemented THY (Figure 8B). However, when supplemented with additional Mn in the growth medium, a drastic 30-fold increase in the intracellular Mn concentration was observed in the Δ*mtsR* mutant strain compared to unsupplemented growth (Figure 8B). Contrarily, only a modest increase in the cytosolic Mn levels was observed in the WT (6.5-fold) and *trans*-complemented (5-fold) strains relative to unsupplemented growth (Figure 8B). Similarly, the Δ*mtsR* mutant strain had elevated intracellular Fe levels (10-fold increase), whereas no or slight increase in the cytosolic Fe levels occurred in the WT or *trans*-complemented strains, respectively (Figure 8B). No major differences in the intracellular Zn concentration was observed among the three strains. Collectively, these data suggest that the increased intracellular Mn and Fe accumulation in the Δ*mtsR* mutant

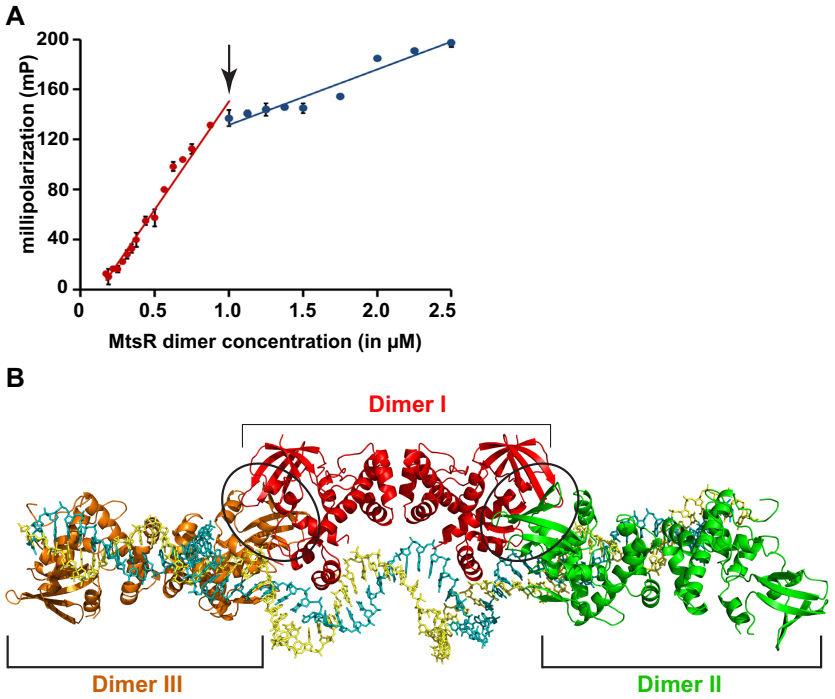

Figure 7. MtsR is engaged in unusual interactions with *mts* motif located in the *mtsA* promoter. (**A**) Fluorescence polarization-based determination of MtsR–*mts* motif binding stoichiometry. Binding of MtsR to the 22 bp *mts* motif sequence as determined by FP assay. The linear fit for the high affinity (specific) and low affinity (non-specific) binding are color coded in red and blue, respectively. The inflection point that denotes the breaking point of high and low-affinity binding are indicated by black arrow. (**B**) Docking studies of the interactions between longer DNA fragment and MtsR multimer. Ribbon representation of crystallographic MtsR oligomer is shown. Three MtsR dimer molecules are shown and each dimer molecule is color coded and labeled (Dimer I–III). The oligomerization interfaces in the FeoA domains of MtsR dimers observed in the crystal structure are circled. The DNA duplex docked on crystallographic MtsR oligomer is shown as sticks and individual strands of the duplex is color coded in cyan and yellow.

likely resulted from constitutive expression of *mtsABC* and *siaABC*.

To determine whether the dysregulation of *mtsABC* and increased cytosolic Mn levels in the *ΔmtsR* mutant increases sensitivity to Mn and affects GAS survival, we compared the growth characteristics of the WT, Δ*mtsR* mutant, and *trans*-complemented (Δ*mtsR:pDC-mtsR*) strains in the presence of increasing concentrations of Mn. In the absence of additional Mn, all three strains had comparable growth kinetics (Figure 8C). Contrarily, when grown in the presence of increasing concentrations of Mn, the Δ*mtsR* mutant was impaired in growth in concert with elevated Mn levels and growth was abolished at 1 mM Mn (Figure 8C). The sensitivity to Mn intoxication in the Δ*mtsR* mutant was reversed to the WT-like phenotype in the *trans*-complemented strain, indicating that the observed growth defect of the Δ*mtsR* mutant strain is due to the inactivation of *mtsR* (Figure 8C). Collectively, these results suggest that the metal-dependent gene regulation by MtsR is critical for the maintenance of optimal intracellular Mn concentration, bacterial survival, and GAS virulence.

DISCUSSION

Pathogenic bacteria encounter a entire spectrum of metal stress conditions ranging from metal deficiency to metal toxicity during different stages of infection (2,8–13,66). Thus, the ability to monitor the alterations in metal levels and evoke stress-specific transcriptional responses is crucial for bacterial survival in the host (12,28,29,67). Here, we report that GAS-encoded transcription regulator MtsR is a Mn-sensing metalloregulator that controls GAS adaptive responses to Mn limitation (Figure 1 and Tables S4-S7). During metal deficiency, MtsR derepresses the transcription of genes involved in Mn acquisition, Fe acquisition, and metal-independent DNA synthesis. Our structural and functional analyses identified two Mn sensing sites in MtsR that monitor Mn availability. Our results suggest that these sites may allow derepression of target gene expression in concert with the severity of Mn deficiency. Finally, our structure-function studies also revealed a novel role for the C-terminal FeoA domain in MtsR oligomerization on target promoters and gene regulation. Importantly, the *mtsR* mutant strains defective in metal sensing and oligomerization were significantly attenuated for GAS virulence, indicating that Mn sensing and stress-specific gene regulation by MtsR are critical events during GAS infection.

GAS primarily upregulates the expression of genes involved in Mn acquisition, Fe import, and metal-independent DNA synthesis for survival during Mn limitation. The contribution of Mn uptake by MtsABC and ribonucleotide synthesis by metal-free NrdEFI.2 to GAS survival under Mn limiting conditions is evident (6,40,68–70). However, it was surprising that GAS induces Fe acquisition in response to Mn limitation. Our data indicate that MtsR senses Mn limitation but upregulates the expression

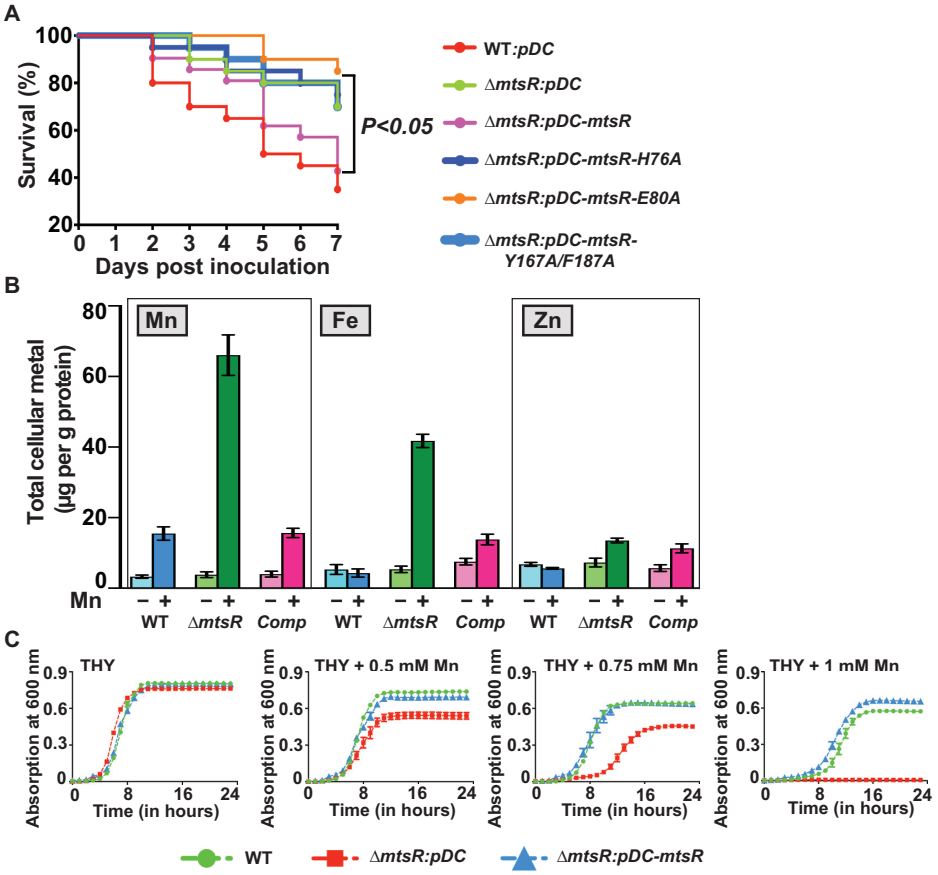

Figure 8. Amino acid residues involved in Mn sensing and oligomerization of MtsR are critical for Mn homeostasis and GAS virulence. (**A**) Twenty outbred CD-1 mice per strain were injected intramuscularly with each indicated strain. Kaplan-Meier survival curve with *P*-values derived by log-rank test is shown. (**B**) The WT, Δ*mtsR*, and *trans*-complemented (*Comp*) strains were grown in THY broth to the mid-exponential phase, incubated with (+) or without (−) 100 μM $MnCl_2$, and the intracellular metal content was measured by ICP-MS. (**C**) Growth kinetics of the indicated strains in THY medium supplemented with increasing concentrations of $MnCl_2$. Growth was monitored by measuring absorption at 600 nm. Three biological replicates were performed, and the graph represents means ± standard deviations.

of both Mn and Fe import machineries. Fe and Mn have pro- and anti-oxidant chemical properties, respectively, and Mn acquisition is a major bacterial strategy to negate the Fe-dependent toxicity of oxidative stress (71–74). As a result, bacteria typically have dedicated sensory and acquisition systems for Mn and Fe, which allows the pathogen to sense and respond in a metal-specific fashion. However, GAS lacks a dedicated Fe-sensing transcription regulator that controls gene expression in response to Fe availability. Thus, despite our *in vitro* results, the possibility that GAS uses MtsR to sense Mn and Fe limitation *in vivo* cannot be ruled out. Consistent with this, Fe caused partial repression of *fhuD.2* and *nrdF.2* genes under the tested conditions, albeit to a lesser degree than Mn, suggesting that Fe has the ability to function as a corepressor for MtsR. Similarly, the metal coordination geometry at site 1 of MtsR appears amenable for Fe binding. In the crystal structure of MtsR, Mn at site 1 is heptacoordinated, an ideal coordination geometry for Mn binding (75). However, Fe could also be accommodated at site 1 of MtsR by hexacoordination and can function as a corepressor. Further structure-function studies will be required to understand the metal selectivity by MtsR, metal-specific allosteric changes in MtsR, metal-specific gene regulation by MtsR, and the *in vivo* relevance of dual metal sensing by MtsR to GAS pathogenesis. An alternate possibility is that lactic acid bacteria such as GAS are Mn-centric organisms and maintain a ≥ 1 Mn:Fe ratio (76–79). In this regard, acquisition of Mn and Fe simultaneously may aid GAS to maintain the ideal intracellular Mn:Fe ratio. Additional investigations are required to fully understand the molecular strategy behind the GAS regulatory mechanism that couples Mn limitation with upregulation of Fe importers.

Structural characterization of Mn-sensing DtxR family regulators has identified several metal sensing sites (20–24). However, with few exceptions, the functional relevance of Mn occupancy at the metal binding sites of DtxR regulators to transcription regulation and bacterial pathogenesis remained unknown. We have identified two metal binding sites in MtsR: metal at site 1 is coordinated by H76, E80, C123, H125 and E160, and site 2 metal is liganded with H32, H95, H161, and D163 (Figures 4 and 5). Metal binding sites analogous to site 1 has been observed in other Mn sensing metalloregulators; however, site 2 in MtsR is distinct from its structural paralogs (Supplementary Figure S9). Nevertheless, we demonstrated that both sites partic-

ipate in Mn sensing and influence the regulatory activity of MtsR, albeit to varying degrees. The metal occupancy at the primary Mn sensing and regulatory site, site 1, is essential for promoter recognition and Mn-dependent gene regulation by MtsR. On the other hand, single alanine substitutions at the metal ligands of the secondary Mn sensing and regulatory site of MtsR caused only partial loss of MtsR-dependent repression of *mtsA*. Based on these observations, we speculate that metal sensing by two sites of MtsR mechanism may enable GAS to fine-tune the degree of *mtsABC* derepression in concert with the severity of Mn deficiency. During Mn sufficiency, both metal binding sites are occupied and MtsR mediates full transcriptional repression of *mtsABC*. When mild Mn deficiency occurs, the loss of metal binding at secondary site, site2, allows GAS to avoid Mn deficiency by partially derepressing *mtsABC* expression. However, during severe Mn limitation, the metal at primary site, site 1, dissociates and the metal-free MtsR mediates complete derepression of *mtsABC* expression, thus allowing GAS to overcome Mn scarcity and survive in Mn sparse environments. Additional mechanistic studies will be required to validate the proposed model.

Another key finding from this study is the role of the C-terminal FeoA domain in MtsR oligomerization and gene regulation. The FeoA domains are observed in most of the DtxR family metalloregulators (20,21,24,62). In DtxR, the FeoA domain interacts with the preceding proline-rich linker that connects the central dimerization domain and FeoA domain (80). Such interactions are critical for the stability of monomeric DtxR (80). However, with the exception of DtxR, other members of the DtxR family lack the long proline-rich linker region and form stable dimers. Thus, the contribution of FeoA domains to transcription regulation by most of the DtxR family regulators remains unknown. We identified an intermolecular interface between the FeoA domains of MtsR dimers that participates in MtsR oligomerization. Consistent with the structural observations, alanine substitutions in the oligomeric interface drastically affected the ability of MtsR to multimerize on *mtsA* promoter sequences, mediate Mn-dependent repression of *mtsA* expression, and cause disease in mouse model of GAS infection. These results suggest that the multimerization of Mn-bound MtsR on the target promoter is a key event in gene regulation. Importantly, the amino acids involved in the FeoA domain interactions and MtsR oligomerization are highly conserved in other Mn-sensing DtxR family regulators (Supplementary Figure S9). However, the amino acids analogous to Y167 and F187 in MtsR are not conserved in Fe-sensing DtxR regulators that are known to bind DNA as dimer of dimers (Supplementary Figure S10). Thus, it is likely that similar intersubunit interactions between FeoA domains of adjacent dimers may occur in other Mn-sensing DtxR family regulators. Consistent with this, multimerization of the regulatory protein on promoter sequences has been observed in other DtxR family regulators (23,57,81,82). Thus, the FeoA domain-dependent oligomerization on the target promoter may be a common regulatory mechanism employed by DtxR regulators to mediate Mn-dependent transcription regulation.

To summarize, the data presented herein suggest a complex sensory mechanism in a metalloregulator that aids the bacteria to efficiently monitor environmental fluctuations in Mn levels and orchestrate gene expression that is optimized for the severity of metal stress. Furthermore, the demonstration of FeoA domain-mediated oligomerization and its contribution to gene regulation in MtsR provides novel insights into the signaling mechanism in DtxR family regulators.

DATA AVAILABILITY

The coordinates and structure factors for the MtsR structure have been deposited to the protein data bank (PDB) with the accession code of 6O5C. Transcriptome data has been deposited in the Gene Expression Omnibus (GEO) under accession code GSE128534.

SUPPLEMENTARY DATA

Supplementary Data are available at NAR Online.

ACKNOWLEDGEMENTS

Author contributions: H.D., N.M., P.C., R.J.O., J.D.H. and M.K. designed and performed research; H.D., N.M., P.C., R.J.O. and M.K. analyzed data; H.D., J.M.M. and M.K. wrote the manuscript.

FUNDING

National Institutes of Health [1R01AI109096-01A1 to M.K.]; Fondren Foundation and National Institutes of Health [AI139369-01A1 to J.M.M., R35GM122461 to J.D.H.]; Advanced Light Source was supported by Department of Energy [DE-AC03-76SF00098]. Funding for open access charge: NIH funding.
Conflict of interest statement. None declared.

REFERENCES

1. Cotruvo,J.A. and Stubbe,J. (2011) *Escherichia coli* Class Ib ribonucleotide reductase contains a Dimanganese(III)-Tyrosyl radical cofactor in vivo. *Biochemistry*, **50**, 1672–1681.
2. Diaz-Ochoa,V.E., Lam,D., Lee,C.S., Klaus,S., Behnsen,J., Liu,J.Z., Chim,N., Nuccio,S.-P., Rathi,S.G., Mastroianni,J.R. *et al.* (2016) Salmonella mitigates oxidative stress and thrives in the inflamed gut by evading calprotectin-mediated manganese sequestration. *Cell Host Microbe.*, **19**, 814–825.
3. Kehl-Fie,T.E., Chitayat,S., Hood,M.I., Damo,S., Restrepo,N., Garcia,C., Munro,K.A., Chazin,W.J. and Skaar,E.P. (2011) Nutrient metal sequestration by calprotectin inhibits bacterial superoxide defense, enhancing neutrophil killing of *Staphylococcus aureus*. *Cell Host Microbe.*, **10**, 158–164.
4. Martin,J.E. and Imlay,J.A. (2011) The alternative aerobic ribonucleotide reductase of Escherichia coli, NrdEF, is a manganese-dependent enzyme that enables cell replication during periods of iron starvation. *Mol. Microbiol.*, **80**, 319–334.
5. Martin,J.E., Lisher,J.P., Winkler,M.E. and Giedroc,D.P. (2017) Perturbation of manganese metabolism disrupts cell division in *Streptococcus pneumoniae*. *Mol. Microbiol.*, **104**, 334–348.
6. Reichardt,W., Gerlach,D. and Vettermann,S. (1998) Extracellular superoxide dismutase from *Streptococcus pyogenes* type 12 strain is manganese-dependent. *FEMS Microbiol. Lett.*, **160**, 217–224.
7. Juttukonda,L.J. and Skaar,E.P. (2015) Manganese homeostasis and utilization in pathogenic bacteria. *Mol. Microbiol.*, **97**, 216–228.

8. Botella,H., Peyron,P., Levillain,F., Poincloux,R., Poquet,Y., Brandli,I., Wang,C., Tailleux,L., Tilleul,S., Charrière,G.M. *et al.* (2011) Mycobacterial P1-Type ATPases mediate resistance to zinc poisoning in human macrophages. *Cell Host Microbe.*, **10**, 248–259.
9. Corbin,B.D., Seeley,E.H., Raab,A., Feldmann,J., Miller,M.R., Torres,V.J., Anderson,K.L., Dattilo,B.M., Dunman,P.M., Gerads,R. *et al.* (2008) Metal chelation and inhibition of bacterial growth in tissue abscesses. *Science*, **319**, 962–965.
10. Damo,S.M., Kehl-Fie,T.E., Sugitani,N., Holt,M.E., Rathi,S., Murphy,W.J., Zhang,Y., Betz,C., Hench,L., Fritz,G. *et al.* (2013) Molecular basis for manganese sequestration by calprotectin and roles in the innate immune response to invading bacterial pathogens. *Proc. Natl. Acad. Sci. U.S.A.*, **110**, 3841–3846.
11. Liu,J.Z., Jellbauer,S., Poe,A.J., Ton,V., Pesciaroli,M., Kehl-Fie,T.E., Restrepo,N.A., Hosking,M.P., Edwards,R.A., Battistoni,A. *et al.* (2012) Zinc sequestration by the neutrophil protein calprotectin enhances salmonella growth in the inflamed gut. *Cell Host & Microbe.*, **11**, 227–239.
12. Makthal,N., Nguyen,K., Do,H., Gavagan,M., Chandrangsu,P., Helmann,J.D., Olsen,R.J. and Kumaraswami,M. (2017) A critical role of zinc importer AdcABC in group A Streptococcus-Host interactions during infection and its implications for vaccine development. *EBioMedicine*, **21**, 131–141.
13. Ong,C.-l.Y., Gillen,C.M., Walker,M.J., Barnett,T.C. and McEwan,A.G. (2014) An antimicrobial role for zinc in innate immune defense against group A streptococcus. *J. Infect. Dis.*, **209**, 1500–1508.
14. Kehl-Fie,T.E., Zhang,Y., Moore,J.L., Farrand,A.J., Hood,M.I., Rathi,S., Chazin,W.J., Caprioli,R.M. and Skaar,E.P. (2013) MntABC and MntH contribute to systemic *Staphylococcus aureus* infection by competing with calprotectin for nutrient manganese. *Infect. Immun.*, **81**, 3395–3405.
15. Huang,X., Shin,J.-H., Pinochet-Barros,A., Su,T.T. and Helmann,J.D. (2017) *Bacillus subtilis* MntR coordinates the transcriptional regulation of manganese uptake and efflux systems. *Mol. Microbiol.*, **103**, 253–268.
16. Haswell,J.R., Pruitt,B.W., Cornacchione,L.P., Coe,C.L., Smith,E.G. and Spatafora,G.A. (2013) Characterization of the functional domains of the SloR metalloregulatory protein in Streptococcus mutans. *J. Bacteriol.*, **195**, 126–134.
17. Johnston,J.W., Briles,D.E., Myers,L.E. and Hollingshead,S.K. (2006) Mn^{2+}-Dependent regulation of multiple genes in *Streptococcus pneumoniae* through PsaR and the resultant impact on virulence. *Infect. Immun.*, **74**, 1171–1180.
18. Reyes-Caballero,H., Campanello,G.C. and Giedroc,D.P. (2011) Metalloregulatory proteins: Metal selectivity and allosteric switching. *Biophys. Chem.*, **156**, 103–114.
19. Merchant,A.T. and Spatafora,G.A. (2014) A role for the DtxR family of metalloregulators in gram-positive pathogenesis. *Mol. Oral Microbiol.*, **29**, 1–10.
20. Feese,M.D., Ingason,B.P., Goranson-Siekierke,J., Holmes,R.K. and Hol,W.G.J. (2001) Crystal structure of the Iron-dependent regulator from *Mycobacterium tuberculosis* at 2.0-Å resolution reveals the Src homology domain 3-like fold and metal binding function of the third domain. *J. Biol. Chem.*, **276**, 5959–5966.
21. Glasfeld,A., Guedon,E., Helmann,J.D. and Brennan,R.G. (2003) Structure of the manganese-bound manganese transport regulator of *Bacillus subtilis*. *Nat. Struct. Biol.*, **10**, 652.
22. Lisher,J.P., Higgins,K.A., Maroney,M.J. and Giedroc,D.P. (2013) Physical characterization of the Manganese-Sensing pneumococcal surface antigen repressor from *Streptococcus pneumoniae*. *Biochemistry*, **52**, 7689–7701.
23. Spatafora,G., Corbett,J., Cornacchione,L., Daly,W., Galan,D., Wysota,M., Tivnan,P., Collins,J., Nye,D., Levitz,T. *et al.* (2015) Interactions of the metalloregulatory protein SloR from *Streptococcus mutans* with its metal ion effectors and DNA binding site. *J. Bacteriol.*, **197**, 3601–3615.
24. Stoll,K.E., Draper,W.E., Kliegman,J.I., Golynskiy,M.V., Brew-Appiah,R.A.T., Phillips,R.K., Brown,H.K., Breyer,W.A., Jakubovics,N.S., Jenkinson,H.F. *et al.* (2009) Characterization and structure of the Manganese-Responsive transcriptional regulator ScaR. *Biochemistry*, **48**, 10308–10320.
25. Cunningham,M.W. (2000) Pathogenesis of Group A Streptococcal infections. *Clin. Microbiol. Rev.*, **13**, 470–511.
26. Ralph,A.P. and Carapetis,J.R. (2013) Group A streptococcal diseases and their global burden. *Curr. Top. Microbiol. Immunol.*, **368**, 1–27.
27. Brunjes Brophy,M., Nakashige,T.G., Gaillard,A. and Nolan,E.M. (2013) Contributions of the S100A9 C-terminal tail to high-affinity Mn(II) chelation by the host-defense protein human calprotectin. *J. Am. Chem. Soc.*, **135**, 17804–17817.
28. Sanson,M., Makthal,N., Flores,A.R., Olsen,R.J., Musser,J.M. and Kumaraswami,M. (2015) Adhesin competence repressor (AdcR) from *Streptococcus pyogenes* controls adaptive responses to zinc limitation and contributes to virulence. *Nucleic Acids Res.*, **43**, 418–432.
29. Makthal,N., Rastegari,S., Sanson,M., Ma,Z., Olsen,R.J., Helmann,J.D., Musser,J.M. and Kumaraswami,M. (2013) Crystal structure of peroxide stress regulator (PerR) from *Streptococcus pyogenes* provides functional insights into the mechanism of oxidative stress sensing. *J. Biol. Chem.*, **288**, 18311–18324.
30. Bates,C.S., Toukoki,C., Neely,M.N. and Eichenbaum,Z. (2005) Characterization of MtsR, a new metal regulator in group A streptococcus, involved in iron acquisition and virulence. *Infect. Immun.*, **73**, 5743–5753.
31. Hanks,T.S., Liu,M., McClure,M.J., Fukumura,M., Duffy,A. and Lei,B. (2006) Differential regulation of Iron- and Manganese-Specific MtsABC and Heme-Specific HtsABC transporters by the metalloregulator MtsR of group A streptococcus. *Infect. Immun.*, **74**, 5132–5139.
32. Lei,B., Liu,M., Voyich,J.M., Prater,C.I., Kala,S.V., DeLeo,F.R. and Musser,J.M. (2003) Identification and characterization of HtsA, a second heme-binding protein made by *Streptococcus pyogenes*. *Infect. Immun.*, **71**, 5962–5969.
33. Lei,B., Smoot,L.M., Menning,H.M., Voyich,J.M., Kala,S.V., Deleo,F.R., Reid,S.D. and Musser,J.M. (2002) Identification and characterization of a novel heme-associated cell surface protein made by *Streptococcus pyogenes*. *Infect. Immun.*, **70**, 4494–4500.
34. Liu,M. and Lei,B. (2005) Heme transfer from streptococcal cell surface protein Shp to HtsA of transporter HtsABC. *Infect. Immun.*, **73**, 5086–5092.
35. Bates,C.S., Montanez,G.E., Woods,C.R., Vincent,R.M. and Eichenbaum,Z. (2003) Identification and characterization of a *Streptococcus pyogenes* operon involved in binding of hemoproteins and acquisition of iron. *Infect. Immun.*, **71**, 1042–1055.
36. Hanks,T.S., Liu,M., McClure,M.J. and Lei,B. (2005) ABC transporter FtsABCD of *Streptococcus pyogenes* mediates uptake of ferric ferrichrome. *BMC Microbiol.*, **5**, 62.
37. Sun,X., Baker,H.M., Ge,R., Sun,H., He,Q.-Y. and Baker,E.N. (2009) Crystal structure and metal Binding properties of the lipoprotein MtsA, responsible for iron transport in *Streptococcus pyogenes*. *Biochemistry*, **48**, 6184–6190.
38. Sun,X., Ge,R., Chiu,J.-F., Sun,H. and He,Q.-Y. (2008) Lipoprotein MtsA of MtsABC in *Streptococcus pyogenes* primarily binds ferrous ion with bicarbonate as a synergistic anion. *FEBS Lett.*, **582**, 1351–1354.
39. Janulczyk,R., Pallon,J. and Björck,L. (1999) Identification and characterization of a Streptococcus pyogenes ABC transporter with multiple specificity for metal cations. *Mol. Microbiol.*, **34**, 596–606.
40. Janulczyk,R., Ricci,S. and Björck,L. (2003) MtsABC is important for manganese and iron transport, oxidative stress resistance, and virulence of *Streptococcus pyogenes*. *Infect. Immun.*, **71**, 2656–2664.
41. Beres,S.B., Carroll,R.K., Shea,P.R., Sitkiewicz,I., Martinez-Gutierrez,J.C., Low,D.E., McGeer,A., Willey,B.M., Green,K. and Tyrrell,G.J. (2010) Molecular complexity of successive bacterial epidemics deconvoluted by comparative pathogenomics. *Proc. Natl. Acad. Sci. U.S.A.*, **107**, 4371–4376.
42. Kuwayama,H., Obara,S., Morio,T., Katoh,M., Urushihara,H. and Tanaka,Y. (2002) PCR-mediated generation of a gene disruption construct without the use of DNA ligase and plasmid vectors. *Nucleic Acids Res.*, **30**, e2.
43. Lukomski,S., Hoe,N.P., Abdi,I., Rurangirwa,J., Kordari,P., Liu,M., Dou,S.-J., Adams,G.G. and Musser,J.M. (2000) Nonpolar inactivation of the hypervariable streptococcal inhibitor of complement gene (*sic*) in serotype M1 *Streptococcus pyogenes* significantly decreases mouse mucosal colonization. *Infect. Immun.*, **68**, 535–542.
44. Sanson,M., O'Neill,B.E., Kachroo,P., Anderson,J.R., Flores,A.R., Valson,C., Cantu,C.C., Makthal,N., Karmonik,C. and Fittipaldi,N. (2015) A naturally occurring single amino acid replacement in

multiple gene regulator of group A Streptococcus significantly increases virulence. *Am. J. Pathol.*, **185**, 462–471.
45. Chaffin,D. and Rubens,C. (1998) Blue/white screening of recombinant plasmids in Gram-positive bacteria by interruption of alkaline phosphatase gene (*phoZ*) expression. *Gene*, **219**, 91–99.
46. Chen,Z., Itzek,A., Malke,H., Ferretti,J.J. and Kreth,J. (2013) Multiple roles of RNase Y in *Streptococcus pyogenes* mRNA processing and degradation. *J. Bacteriol.*, **195**, 2585–2594.
47. Virtaneva,K., Porcella,S.F., Graham,M.R., Ireland,R.M., Johnson,C.A., Ricklefs,S.M., Babar,I., Parkins,L.D., Romero,R.A., Corn,G.J. *et al.* (2005) Longitudinal analysis of the group A Streptococcus transcriptome in experimental pharyngitis in cynomolgus macaques. *Proc. Natl. Acad. Sci. U.S.A.*, **102**, 9014–9019.
48. Leslie,A. (2006) The integration of macromolecular diffraction data. *Acta Crystallogr. D*, **62**, 48–57.
49. Collaborative. (1994) The CCP4 suite: programs for protein crystallography. *Acta Crystallogr. D*, **50**, 760–763.
50. Emsley,P. and Cowtan,K. (2004) Coot: model-building tools for molecular graphics. *Acta Crystallogr. D Biol. Crystallogr.*, **60**, 2126–2132.
51. Adams,P.D., Afonine,P.V., Bunkoczi,G., Chen,V.B., Davis,I.W., Echols,N., Headd,J.J., Hung,L.-W., Kapral,G.J., Grosse-Kunstleve,R.W. *et al.* (2010) PHENIX: a comprehensive Python-based system for macromolecular structure solution. *Acta Crystallogr. D*, **66**, 213–221.
52. Chen,V.B., Arendall,W.B. 3rd, Headd,J.J., Keedy,D.A., Immormino,R.M., Kapral,G.J., Murray,L.W., Richardson,J.S. and Richardson,D.C. (2010) MolProbity: all-atom structure validation for macromolecular crystallography. *Acta Crystallogr. D Biol. Crystallogr.*, **66**, 12–21.
53. Davis,I.W., Leaver-Fay,A., Chen,V.B., Block,J.N., Kapral,G.J., Wang,X., Murray,L.W., Arendall,W.B. 3rd, Snoeyink,J., Richardson,J.S. *et al.* (2007) MolProbity: all-atom contacts and structure validation for proteins and nucleic acids. *Nucleic Acids Res.*, **35**, W375–W383.
54. DeLano,W.L. (2002) *The PyMol Molecular Graphics System*. DeLano Scientific, Palo Alto.
55. Olsen,R.J., Sitkiewicz,I., Ayeras,A.A., Gonulal,V.E., Cantu,C., Beres,S.B., Green,N.M., Lei,B., Humbird,T., Greaver,J. *et al.* (2010) Decreased necrotizing fasciitis capacity caused by a single nucleotide mutation that alters a multiple gene virulence axis. *Proc. Natl. Acad. Sci. U.S.A.*, **107**, 888–893.
56. Beres,S.B., Richter,E.W., Nagiec,M.J., Sumby,P., Porcella,S.F., DeLeo,F.R. and Musser,J.M. (2006) Molecular genetic anatomy of inter- and intraserotype variation in the human bacterial pathogen group A Streptococcus. *Proc. Natl. Acad. Sci. U.S.A.*, **103**, 7059–7064.
57. Toukoki,C., Gold,K.M., McIver,K.S. and Eichenbaum,Z. (2010) MtsR is a dual regulator that controls virulence genes and metabolic functions in addition to metal homeostasis in the group A streptococcus. *Mol. Microbiol.*, **76**, 971–989.
58. Grifantini,R., Toukoki,C., Colaprico,A. and Gryllos,I. (2011) Peroxide stimulon and role of PerR in group A streptococcus. *J. Bacteriol.*, **193**, 6539–6551.
59. Kaatz,G.W., Schuman,J.T., Kumaraswami,M., Seo,S.M. and Brennan,R.G. (2009) Structural and biochemical characterization of MepR, a multidrug binding transcription regulator of the *Staphylococcus aureus* multidrug efflux pump MepA. *Nucleic Acids Res.*, **37**, 1211–1224.
60. Huffman,J.L. and Brennan,R.G. (2002) Prokaryotic transcription regulators: more than just the helix-turn-helix motif. *Curr. Opin. Struct. Biol.*, **12**, 98–106.
61. Connolly,M. (1983) Solvent-accessible surfaces of proteins and nucleic acids. *Science*, **221**, 709–713.
62. Cong,X., Yuan,Z., Wang,Z., Wei,B., Xu,S. and Wang,J. (2018) Crystal structures of manganese-dependent transcriptional repressor MntR (Rv2788) from *Mycobacterium tuberculosis* in apo and manganese bound forms. *Biochem. Biophys. Res. Commun.*, **501**, 423–427.
63. Pohl,E., Holmes,R.K. and Hol,W.G.J. (1999) Crystal structure of a Cobalt-activated diphtheria toxin Repressor-DNA complex reveals a Metal-binding SH3-like domain. *J. Mol. Biol.*, **292**, 653–667.
64. Wisedchaisri,G., Holmes,R.K. and Hol,W.G.J. (2004) Crystal structure of an IdeR–DNA complex reveals a conformational change in activated IdeR for Base-specific interactions. *J. Mol. Biol.*, **342**, 1155–1169.
65. Schumacher,M.A., den Hengst,C.D., Bush,M.J., Le,T.B.K., Tran,N.T., Chandra,G., Zeng,W., Travis,B., Brennan,R.G. and Buttner,M.J. (2018) The MerR-like protein BldC binds DNA direct repeats as cooperative multimers to regulate Streptomyces development. *Nat. Commun.*, **9**, 1139.
66. Stähler,F.N., Odenbreit,S., Haas,R., Wilrich,J., Vliet,A.H.M.V., Kusters,J.G., Kist,M. and Bereswill,S. (2006) The Novel H*elicobacter pylori* CznABC metal efflux pump is required for cadmium, zinc, and nickel resistance, urease modulation, and gastric colonization. *Infect. Immun.*, **74**, 3845–3852.
67. VanderWal,A.R., Makthal,N., Pinochet-Barros,A., Helmann,J.D., Olsen,R.J. and Kumaraswami,M. (2017) Iron efflux by PmtA is critical for oxidative stress resistance and contributes significantly to group A Streptococcus virulence. *Infect. Immun.*, **85**, e00091-17.
68. Turner,A.G., Djoko,K.Y., Ong,C.-l.Y., Barnett,T.C., Walker,M.J. and McEwan,A.G. (2019) Group A *Streptococcus* co-ordinates manganese import and iron efflux in response to hydrogen peroxide stress. *Biochem. J.*, **476**, 595–611.
69. Roca,I., Torrents,E., Sahlin,M., Gibert,I. and Sjöberg,B.-M. (2008) NrdI essentiality for class Ib ribonucleotide reduction in *Streptococcus pyogenes*. *J. Bacteriol.*, **190**, 4849–4858.
70. Blaesi,E.J., Palowitch,G.M., Hu,K., Kim,A.J., Rose,H.R., Alapati,R., Lougee,M.G., Kim,H.J., Taguchi,A.T., Tan,K.O. *et al.* (2018) Metal-free class Ie ribonucleotide reductase from pathogens initiates catalysis with a tyrosine-derived dihydroxyphenylalanine radical. *Proc. Natl. Acad. Sci. U.S.A.*, **115**, 10022–10027.
71. Lee,J.-W. and Helmann,J.D. (2006) The PerR transcription factor senses H_2O_2 by metal-catalysed histidine oxidation. *Nature*, **440**, 363.
72. Anjem,A. and Imlay,J.A. (2012) Mononuclear iron enzymes are primary targets of hydrogen peroxide stress. *J. Biol. Chem.*, **287**, 15544–15556.
73. Gu,M. and Imlay,J.A. (2013) Superoxide poisons mononuclear iron enzymes by causing mismetallation. *Mol. Microbiol.*, **89**, 123–134.
74. Imlay,J.A. (2013) The molecular mechanisms and physiological consequences of oxidative stress: lessons from a model bacterium. *Nat. Rev. Microbiol.*, **11**, 443.
75. Bachas,S.T. and Ferré-D'Amaré,A.R. (2018) Convergent use of heptacoordination for cation selectivity by RNA and protein metalloregulators. *Cell Chem. Biol.*, **25**, 962–973.
76. Lisher,J.P. and Giedroc,D.P. (2013) Manganese acquisition and homeostasis at the host-pathogen interface. *Front. Cell Infect. Microbiol.*, **3**, 91.
77. Daly,M.J., Gaidamakova,E.K., Matrosova,V.Y., Vasilenko,A., Zhai,M., Venkateswaran,A., Hess,M., Omelchenko,M.V., Kostandarithes,H.M., Makarova,K.S. *et al.* (2004) Accumulation of Mn(II) in *Deinococcus radiodurans* facilitates gamma-radiation resistance. *Science*, **306**, 1025–1028.
78. Jacobsen,F.E., Kazmierczak,K.M., Lisher,J.P., Winkler,M.E. and Giedroc,D.P. (2011) Interplay between manganese and zinc homeostasis in the human pathogen *Streptococcus pneumoniae*. *Metallomics*, **3**, 38–41.
79. Veyrier,F.J., Boneca,I.G., Cellier,M.F. and Taha,M.-K. (2011) A novel metal transporter mediating manganese export (MntX) regulates the Mn to Fe intracellular ratio and *Neisseria meningitidis* virulence. *PLoS Pathog.*, **7**, e1002261.
80. Wylie,G.P., Rangachari,V., Bienkiewicz,E.A., Marin,V., Bhattacharya,N., Love,J.F., Murphy,J.R. and Logan,T.M. (2005) Prolylpeptide binding by the prokaryotic SH3-like domain of the diphtheria toxin Repressor: a regulatory switch. *Biochemistry*, **44**, 40–51.
81. Jakubovics,N.S., Smith,A.W. and Jenkinson,H.F. (2000) Expression of the virulence-related Sca (Mn2+) permease in *Streptococcus gordonii* is regulated by a diphtheria toxin metallorepressor-like protein ScaR. *Mol. Microbiol.*, **38**, 140–153.
82. Pandey,R., Russo,R., Ghanny,S., Huang,X., Helmann,J. and Rodriguez,G.M. (2015) MntR(Rv2788): a transcriptional regulator that controls manganese homeostasis in *Mycobacterium tuberculosis*. *Mol. Microbiol.*, **98**, 1168–1183.